Journal of Molecular Structure 1141 (2017) 495–511

Contents lists available at ScienceDirect

Journal of Molecular Structure

journal homepage: http://www.elsevier.com/locate/molstruc

Modification of benzoxazole derivative by bromine-spectroscopic, antibacterial and reactivity study using experimental and theoretical procedures

V.V. Aswathy [a], Sabiha Alper-Hayta [b], Gözde Yalcin [c], Y. Sheena Mary [a, *], C. Yohannan Panicker [a], P.J. Jojo [a], Fatma Kaynak-Onurdag [d], Stevan Armaković [e], Sanja J. Armaković [f], Ilkay Yildiz [g], C. Van Alsenoy [h]

[a] Department of Physics, Fatima Mata National College, Kollam, Kerala, India
[b] Republic of Turkey Ministry of Health, Turkish Medicines and Medical Devices Agency, 2176 Str. Söğütözü, 06520 Çankaya, Ankara, Turkey
[c] Ankara University, Biotechnology Institute, Tandogan 06100, Ankara, Turkey
[d] Trakya University, Faculty of Pharmacy, Department of Pharmaceutical Microbiology, 22030 Balkan Yerleskesi, Edirne, Turkey
[e] University of Novi Sad, Faculty of Sciences, Department of Physics, Trg D. Obradovića 4, 21000 Novi Sad, Serbia
[f] University of Novi Sad, Faculty of Sciences, Department of Chemistry, Biochemistry and Environmental Protection, Trg D. Obradovića 3, 21000 Novi Sad, Serbia
[g] Ankara University, Faculty of Pharmacy, Department of Pharmaceutical Chemistry, 06100 Tandogan, Ankara, Turkey
[h] Department of Chemistry, University of Antwerp, Groenenborgerlaan 171, B-2020, Antwerp, Belgium

ARTICLE INFO

Article history:
Received 29 September 2016
Received in revised form
1 April 2017
Accepted 3 April 2017
Available online 6 April 2017

Keywords:
Benzoxazole
ALIE
RDF
BDE
Moleculardocking
Antibacterial activity

ABSTRACT

N-[2-(2-bromophenyl)-1,3-benzoxazol-5-yl]-2-phenylacetamide (NBBPA) was synthesized in this study as an original compound in order to evaluate its antibacterial activity against representative Gram-negative and Gram-positive bacteria, with their drug-resistant clinical isolate. Microbiological results showed that this compound had moderate antibacterial activity. Study also encompassed detailed FT-IR, FT-Raman and NMR experimental and theoretical spectroscopic characterization and assignation of the ring breathing modes of the mono-, ortho- and tri-substituted phenyl rings is in agreement with the literature data. DFT calculations were also used to identify specific reactivity properties of NBBPA molecule based on the molecular orbital, charge distribution and electron density analysis, which indicated the reactive importance of carbonyl and NH_2 groups, together with bromine atom. DFT calculations were also used for investigation of sensitivity of the NBBPA molecules towards the autoxidation mechanism, while molecular dynamics (MD) simulations were used to investigate the influence of water. The molecular docking results suggest that the compound might exhibit inhibitory activity against GyrB complex.

1. Introduction

Benzoxazole ring is one of the most common heterocycles in medicinal chemistry. Previous reports revealed that substituted benzoxazoles possess diverse chemotherapeutic activities including antimicrobial [1–5], antiviral [6], topoisomerase I and II inhibitors [7] and antitumor activities [8,9]. Bacterial resistance to antibacterial agents or antibiotics is of grave concern in the medical community, as many species of bacteria have evolved resistance to certain antibiotics and synthetic agents. Therefore, there could be a rapidly growing global crisis in the clinical management of life-threatening infectious diseases caused by multidrug-resistant strains of the Gram-positive pathogens like Streptococcus, Enterococcus, and Staphylococcus, and Gram-negative pathogens like Escherichia, Salmonella, and certain Pseudomonas strains. Especially the emergence of multidrug-resistant strains of Gram-positive bacterial pathogens such as methicillin-resistant *Staphylococcus aureus* and *Staphylococcus epidermis* and vancomycin-resistant Enterococcus is an alarming problem of ever increasing significance [10–12]. To meet this crisis successfully, many researchers across the globe are working to unearth new compounds

* Corresponding author.
E-mail address: sypanicker@rediffmail.com (Y.S. Mary).

http://dx.doi.org/10.1016/j.molstruc.2017.04.010
0022-2860/

which can selectively attack novel targets in microorganisms. Hence, the development of novel, potent, and unique antibacterial agents is the preeminent way to overcome bacterial resistance and develop effective therapies [13]. In previous studies, we synthesized some compounds which bearing a hydrogen, chlorine, methyl, nitro, an amine, ester, and amide substitution at the 5th position on the benzoxazole ring and examined for their *in vitro* antimicrobial activity against some Gram-positive, Gram-negative bacteria and *Candida albicans* [1–3,14,15]. On the basis of these considerations, we synthesized *N*-[2-(2-bromophenyl)-1,3-benzoxazol-5-yl]-2-phenylacetamide (NBBPA) as antimicrobial agent reported in this work, choosing a bromine atom at the 2nd position of phenyl of second carbon of benzoxazole ring. The strategy employed was to examine the effect of the bromine against some Gram-positive, Gram-negative bacteria and their drug-resistant isolates.

One of the main characteristics of biologically active molecules is their overall stability, especially in aquatic mediums. These organic molecules are synthesized to be highly stable, which hardens their removal from the water and soil [16]. Since pharmaceutical care products are frequently used and improperly dumped into the environment their active components accumulate in water, which is very harmful because it has been shown that aforementioned molecules exhibit toxic effects towards aquatic organisms [16,17]. The fact that biologically active molecules that serve as active components of pharmaceutical products have been detected in all types of water is particularly upsetting, since conventional methods for the removal of these molecules are ineffective [18,19]. Removal of these molecules based on forced degradation by advanced oxidation processes could be fine alternative [17,18,20,21] and it also might serve as a basis for the studies of their toxic effects [22–24]. Rationalization of studies based on forced degradation can be done by application of DFT calculations and MD simulations [25–27]. Principles of molecular modeling enable prediction of reactive properties of investigated molecules, further influencing the improvement and development of procedures for the purification of water. Bearing in mind the usefulness of theoretical analysis, in this work we have investigated reactivity in order to gain an insight into the possible degradation properties of NBBPA molecule.

2. Experimental section

2.1. Synthesis of N-[2-(2-bromophenyl)-1,3-benzoxazol-5-yl]-2-phenylacetamide

The firstly synthesis of *N*-[2-(2-bromophenyl)-1,3-benzoxazol-5-yl]-2-phenylacetamide was obtained in two step procedures as given below (Scheme 1):

First step: 5-Amino-2-(2-bromophenyl) benzoxazole was synthesized by heating 0.01 mol 2,4-diaminophenol.2HCl with 0.01 mol 2-bromobenzoic acid in 12.5 g polyphosphoric acid (PPA) and stirring at 200 °C for 4 h. At the end of the reaction period, the residue was poured into ice water mixture and neutralized with excess of 10 M NaOH solution extracted with benzene and then this solution was dried over anhydrous sodium sulphate and evaporated under diminished pressure. The residue was boiled with 200 mg charcoal in ethanol and filtered. After the evaporation of solvent *in vacuo*, the crude product was obtained and recrystallized from ethanol.

Second step: Phenylacetic acid (0.5 mmol) and thionyl chloride (1.5 ml) were refluxed in benzene (5 ml) at 80 °C for 3 h. Excess thionyl chloride was removed *in vacuo*. The residue was dissolved in ether (10 ml) and this solution was added during 1 h to a stirred, ice-cold mixture of 5-amino-2-(2-bromophenyl)benzoxazole (0.5 mmol), sodium bicarbonate (0.5 mmol), diethyl ether (10 ml) and water (10 ml). The mixture was kept stirred overnight at room temperature and filtered. The precipitate was washed with water, 2 N HCl and water and finally with ether to give *N*-[2-(2-bromophenyl)-1,3-benzoxazol-5-yl]-2-phenylacetamide. The product was recrystallized from ethanol-water as needles, which was dried *in vacuo*. The chemical, physical and spectral data of the compound are reported below; $C_{21}H_{15}BrN_2O_2.1{,}75H_2O$, yield: 61,42%, mp: 145–147 °C. MS (70 eV) *m/z*: 429 (M^++H+23(Na)), 431 (M^++H+2 + 23(Na)). Elemental Analysis: Calculated: C: 57.48, H: 4.25, N:6.38; Found: C: 57.19, H: 3.92, N: 6.32.

The chemicals were purchased from the commercial venders and were used without purification. The reactions were monitored and the purity of the products was checked by thin layer chromatography TLC. Kieselgel HF 254 chromatoplates (0.3 mm) was used for TLC and the solvent system was ethylacetate:n-hexane (2:1). The melting point was taken on a Buchi SMP 20 capillary apparatus and is uncorrected. ^{1}H NMR spectra was obtained with a Varian 400 MHz spectrometer in dimethylsulfoxide-d6 (DMSO-d_6) and tetramethylsilane (TMS) was used as an internal standard. Mass analyses was carried out with a Waters Micromass ZQ by using ESI^+ method. Elemental analysis was performed on LECO 932 CHNS (Leco 932, St. Joseph, MI, USA) instrument and was within 0.4% of the theoretical values. All chemicals and solvents were purchased from Aldrich Chemical Co. or Fischer Scientific.

The FT-IR spectrum (Fig. 1) was recorded using KBr pellets on a DR/Jasco FT-IR 6300 spectrometer. The FT-Raman spectrum (Fig. 2) was obtained on a Bruker RFS 100/s, Germany. For excitation of the spectrum the emission of Nd:YAG laser was used, excitation wavelength 1064 nm, maximal power 150 mW, measurement on solid sample. The spectral resolution after apodization was 2 cm^{-1}.

2.2. Microbiology

Microorganisms *Pseudomonasaeruginosa* isolate (gentamicin-resistant), *Escherichiacoli* isolate, which has an extended spectrum beta lactamase enzyme (ESBL), *Staphylococcus aureus* isolate (meticilline-resistant (MRSA)), *P. aeruginosa* ATCC 27853 (American Type Culture Collection), *E. coli* ATCC 25922, *S. aureus* ATCC 29213, *Enterococcus faecalis* ATCC 29212, *E. faecalis* isolate (vancomycin-resistant enterococci). Methods Standard strains of *P. aeruginosa* ATCC 25853, *E. coli* ATCC 25922, *S. aureus* ATCC 25923, *E. faecalis* ATCC 29212 and clinical isolates of these microorganisms resistant to various antimicrobial agents were included in the study. Resistance was determined by Kirby Bauer Disk Diffusion method according to the guidelines of Clinical and Laboratory Standards Institute (CLSI) [28] in the clinical isolates. Standard powders of ampicillin trihydrate, gentamycin sulphate, ofloxacin were obtained from the manufacturers. Stock solutions were dissolved in dimethylsulphoxide (ofloxacin), pH 8 phosphate buffer saline (PBS) (ampicillin trihydrate) and distilled water (gentamicin sulphate). Newly synthesized compound was dissolved in 80% DMSO-20% EtOH. Bacterial isolates were subcultured in Mueller Hinton Agar (MHA) plates and incubated over night at 37 °C for 24–48 h. The microorganisms were passaged at least twice to ensure purity and viability. The solution of the newly synthesized compound and standard drugs were prepared at 400, 200, 100, 50, 25, 12.5, 6.25, 3.125, 1.562, 0.78, 0.39, 0.19, 0.095, 0.047, 0.024 μg/ml concentrations, in the wells of microplates by diluting in Mueller Hinton Broth (MHB). Bacterial susceptibility testing was performed according to the guidelines of CLSI M100-S16 [29].

The bacterial suspensions used for inoculation were prepared at 10^5 cfu/ml by diluting fresh cultures at MacFarland 0.5 density (10^7 cfu/ml). Suspensions of the bacteria at 10^5 cfu/ml concentration were inoculated to the twofold diluted solution of the

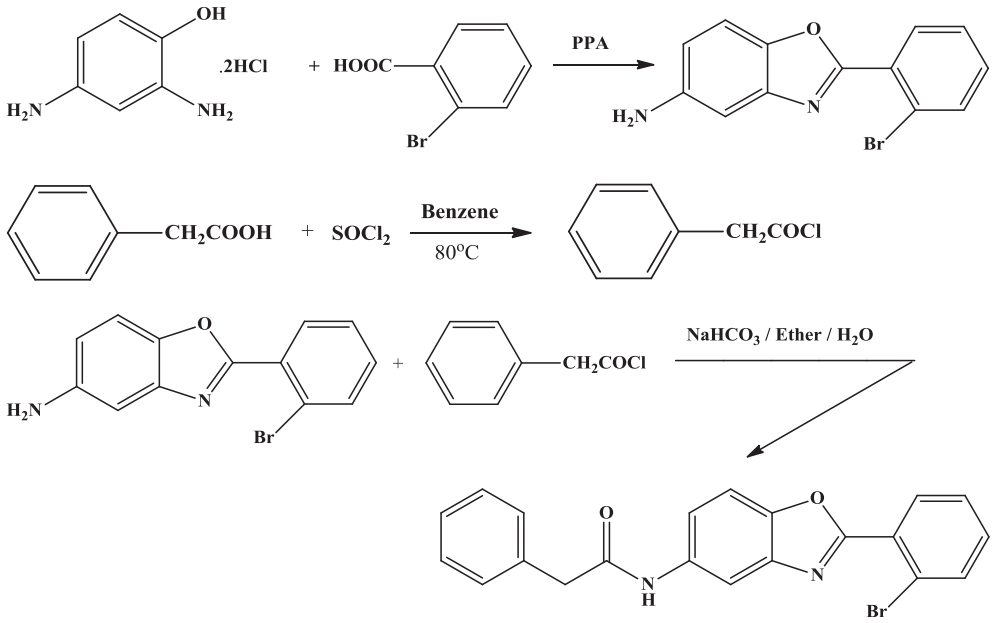

Scheme 1. Synthetic pathway of *N*-[2-(2-bromophenyl)-1,3-benzoxazol-5-yl]-2-phenylacetamide.

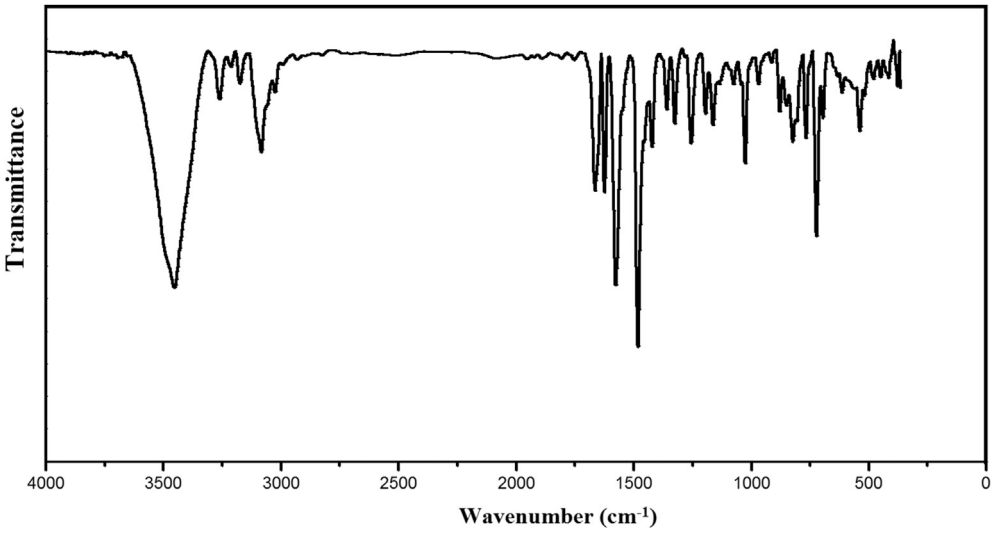

Fig. 1. FT-IR spectrum of *N*-[2-(2-bromophenyl)-1,3-benzoxazol-5-yl]-2-phenylacetamide.

compounds. There were 10^4 cfu/ml bacteria in the wells after inoculations. MHB was used for diluting the bacterial suspension and for twofold dilution of the compound. 80% DMSO-20% EtOH, methanol, DMSO, PBS, pure microorganisms and pure media were used as control wells. A 10 μl bacteria inoculum was added to each well of the microdilution trays. The trays were incubated at 37 °C and MIC endpoints were read after 24 h of incubation. All organisms were tested in triplicate in each run of the experiments. The lowest concentration of the compound that completely inhibits macroscopic growth was determined and minimum inhibitory concentrations (MICs) were reported in Table 1.

3. Computational details

Calculations of the wavenumbers, NMR chemical shifts, MEP and NBO analysis of the NBBPA molecule are carried out with Gaussian09 program [30] using B3LYP/6-311++G (5D, 7F) quantum chemical calculations method. A scaling factor of 0.9613 is used to scale the theoretically predicted wavenumbers [31]. The assignments of the wavenumbers are done by using GaussView [32] and GAR2PED [33] software. The theoretically predicted geometrical parameters (Fig. 3) are given in Table 2.

In this work Schrödinger Materials Science Suite 2015-4 has been also employed for the DFT calculations and MD simulations. Desmond program was used for MD simulations [34–37], while Jaguar 9.0 program [38] was used for DFT calculations. Calculations performed with Jaguar were done with B3LYP exchange-correlation functional [39], together with 6–311++G(d,p), 6-31 + G(d,p) and 6-311G(d,p) basis sets for the calculations of ALIE, Fukui functions and BDEs, respectively. OPLS 2005 force field [40] was used in case of MD simulations with Desmond program. Simulation time was set to 10 ns, within isothermal–isobaric (NPT) ensemble class. To model the interactions with water one NBBPA molecule was placed in cubic box with ~3000 water molecules. Temperature was set to

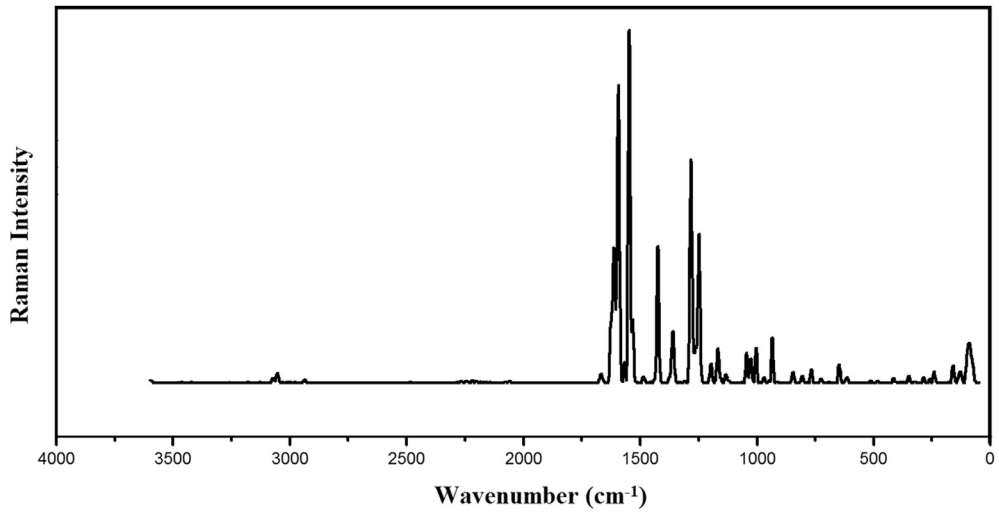

Fig. 2. FT-Raman spectrum of *N*-[2-(2-bromophenyl)-1,3-benzoxazol-5-yl]-2-phenyl acetamide.

Table 1
The microbiological result of *N*-[2-(2-bromophenyl)-1,3-benzoxazol-5-yl]-2-phenylacetamide.

Compounds	Microorganisms (MIC value, μg/ml)							
	Gram-negative				Gram-positive			
	E.c	E.c*	P.a.	P.a.*	S.a.	S.a.*	E.f.	E.f.*
Title compound	128	128	64	128	128	64	32	128
Ampicillin	2	>1024	–	–	0.5	–	0.5	0.5
Ofloxacine	0.015	16	1	1	0.125	0.5	1	4
Gentamycin	0.25	256	1	64	0.5	128	8	8

Abbreviations: ***E.c****:Escherichia coli*ATCC 25922**, E.c*:***Escherichiacoli**isolate, which has an extended spectrum beta lactamase enzyme (ESBL), ***P.a***: *Pseudomonas aeruginosa* ATCC 27853 (American Type Culture Collection),***P.a****: *Pseudomonas aeruginosa*isolate (gentamicin-resistant), ***S.a***: *Staphylococcus. aureus* ATCC 29213,***S.a****:*Staphylococcus aureus* isolate [meticilline-resistant (MRSA)], ***E.f***: *Enterococcus faecalis* ATCC 29212, ***E.f****: *Enterecoccus faecalis* isolate (vancomycin-resistant enterococci).

300 K, pressure set to 1.0325 bar, cut off radius to 12 Å. Simple point charge (SPC) model [41] was used for the treatment of solvent. Noncovalent interactions in Jaguar program are treated by the method developed by Johnson et al. [42,43]. Maestro GUI [44] was used for the preparation of input files and analysis of results when Schrödinger Materials Science Suite 2015–4 was used.

4. Results and discussion

4.1. Chemistry

For the synthesis of NBBPA firstly, 5-amino-2-(*p*-bromophenyl) benzoxazole was obtained by heating 2-bromobenzoic acid with 2,4-diaminophenol in PPA. *N*-[2-(2-bromophenyl)-1,3-benzoxazol-5-yl]-2-phenylacetamide was obtained from 5-amino-2-(*p*-bromophenyl)benzoxazole with phenylacetylchloride obtained by

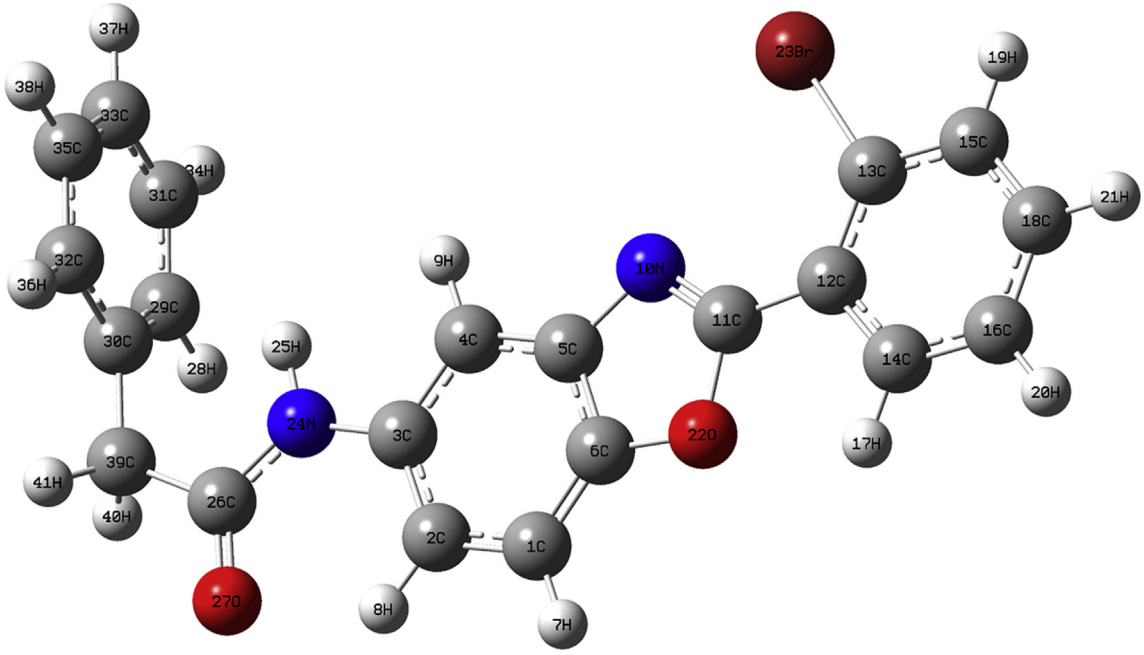

Fig. 3. Optimized geometry of *N*-[2-(2-bromophenyl)-1,3-benzoxazol-5-yl]-2-phenyl acetamide.

Table 2
Optimized geometrical parameters.

Bond lengths (Á)					
C1–C2	1.3987	C1–C6	1.3830	C1–H7	1.0799
C2–C3	1.4168	C2–H8	1.0765	C3–C4	1.4042
C3–N24	1.4198	C4–C5	1.3906	C4–H9	1.0818
C5–C6	1.4004	C5–N10	1.4103	C6–O22	1.3988
N10–C11	1.3080	C11–C12	1.4558	C11–O22	1.4273
C12–C13	1.4102	C12–C14	1.4145	C13–C15	1.3956
C13–Br23	1.9469	C14–C16	1.3889	C14–H17	1.0788
C15–C18	1.3942	C15–H19	1.0795	C16–C18	1.3972
C16–H20	1.0813	C18–H21	1.0817	N24–H25	1.0102
N24–C26	1.3708	C26–O27	1.2509	C26–C39	1.5352
H28–C29	1.0835	C29–C30	1.4055	C29–C31	1.3978
C30–C32	1.4055	C30–C39	1.5130	C31–C33	1.3982
C31–H34	1.0822	C32–C35	1.3978	C32–H36	1.0835
C33–C35	1.3982	C33–H37	1.0819	C35–H38	1.0822
C39–H40	1.0924	C39–H41	1.0923		
Bond angles (°)					
C2–C1–C6	116.9	C2–C1–H7	120.9	C6–C1–H7	122.2
C1–C2–C3	121.0	C1–C2–H8	120.3	C3–C2–H8	118.7
C2–C3–C4	120.9	C2–C3–N24	122.4	C4–C3–N24	116.7
C3–C4–C5	117.8	C3–C4–H9	121.7	C5–C4–H9	120.5
C4–C5–C6	120.4	C4–C5–N10	130.5	C6–C5–N10	109.1
C1–C6–C5	123.0	C1–C6–O22	129.5	C5–C6–O22	107.5
C5–N10–C11	106.1	N10–C11–C12	131.5	N10–C11–O22	113.0
C12–C11–O22	115.5	C11–C12–C13	125.2	C11–C12–C14	117.4
C13–C12–C14	117.4	C12–C13–C5	120.7	C12–C13–Br23	123.7
C15–C13–Br23	115.6	C12–C14–C16	121.8	C12–C14–H17	118.1
C16–C14–H17	120.1	C13–C15–C18	120.7	C13–C15–H19	119.0
C18–C15–H19	120.3	C14–C16–C18	119.7	C14–C16–H20	119.8
C18–C16–H20	120.5	C15–C18–C16	119.6	C15–C18–H21	119.6
C16–C18–H21	120.7	C6–O22–C11	104.3	C3–N24–H25	115.1
C3–N24–C26	129.3	H25–N24–C26	115.6	N24–C26–O27	124.1
N24–C26–C39	116.4	O27–C26–C39	119.5	H28–C29–C30	119.4
H28–C29–C31	119.7	C30–C29–C31	120.8	C29–C30–C32	118.4
C29–C30–C39	120.8	C32–C30–C39	120.8	C29–C31–C33	120.1
C29–C31–H34	119.8	C33–C31–H34	120.1	C30–C32–C35	120.8
C30–C32–H36	119.4	C35–C32–H36	119.7	C31–C33–C35	119.7
C31–C33–H37	120.2	C35–C33–H37	120.2	C32–C35–C33	120.1
C32–C35–H38	119.8	C33–C35–H38	120.1	C26–C39–C30	117.7
C26–C39–H40	105.7	C26–C39–H41	105.7	C30–C39–H40	110.5
C30–C39–H41	110.5	H40–C39–H41	105.9		
Dihedral angles (°)					
C6–C1–C2C3	0.0	C6–C1–C2–H8	−180.0	H7–C1–C2–C3	180.0
H7–C1–C2–H8	0.0	C2–C1–C6–C5	0.0	C2–C1–C6–O22	180.0
H7–C1–C6–C5	−180.0	H7–C1–C6–O22	0.0	C1–C2–C3–C4	0.0
C1–C2–C3–N24	180.0	H8–C2–C3–C4	180.0	H8–C2–C3–N24	−0.0
C2–C3–C4–C5	0.0	C2–C3–C4–H9	−180.0	N24–C3–C4–C5	−180.0
N24–C3–C4–H9	0.0	C2–C3–N24–H25	−180.0	C2–C3–N24–C26	0.0
C4–C3–N24–H25	0.0	C4–C3–N24–C26	−180.0	C3–C4–C5–C6	0.0
C3–C4–C5–N10	180.0	H9–C4–C5–C6	180.0	H9–C4–C5–N10	0.0
C4–C5–C6–C1	0.0	C4–C5–C6–O22	−180.0	N10–C5–C6–C1	180.0
N10–C5–C6–O22	0.0	C4–C5–N10–C11	180.0	C6–C5–N10–C11	0.0
C1–C6–O22–C11	−180.0	C5–C6–O22–C11	0.0	C5–N10–C11–C12	−180.0
C5–N10–C11–C22	0.0	N10–C11–C12–C13	−0.0	N10–C11–C12–C14	180.0
O22–C11–C12–C13	180.0	O22–C11–C12–C14	−0.0	N10–C11–O22–C6	0.0
C12–C11–O22–C6	180.0	C11–C12–C13–C15	−180.0	C11–C12–C13–Br23	0.0
C14–C12–C13–C15	0.0	C14–C12–C13–Br23	180.0	C11–C12–C14–C16	180.0
C11–C12–C14–H17	0.0	C13–C12–C14–C16	−0.0	C13–C12–C14–H17	−180.0
C12–C13–C15–C18	0.0	C12–C13–C15–H19	180.0	Br23–C13–C15–C18	−180.0
Br23–C13–C15–H19	0.0	C12–C14–C16–C18	−0.0	C12–C14–C16–H20	180.0
H17–C14–C16–C18	−180.1	H17–C14–C16–H20	0.0	C13–C15–C18–C16	−0.0
C13–C15–C18–H21	180.0	H19–C15–C18–C16	−180.0	H19–C15–C18–H21	0.0
C14–C16–C18–C15	0.0	C14–C16–C18–H21	−180.0	H20–C16–C18–C15	180.0
H20–C16–C18–H21	−0.0	C3–N24–C26–O27	0.0	C3–N24–C26–C39	−180.0
H25–N24–C26–O27	−180.0	H25–N24–C26–C39	0.0	N24–C26–C39–C30	−0.1
N24–C26–C39–H40	123.9	N24–C26–C39–H41	−124.1	O27–C26–C39–C30	179.9
O27–C26–C39–H40	−56.1	O27–C26–C39–H41	55.9	H28–C29–C30–C32	−179.3
H28–C29–C30–C39	1.1	C31–C29–C30–C32	0.5	C31–C29–C30–C39	−179.1
H28–C29–C31–C33	179.6	H28–C29–C31–H34	0.0	C30–C29–C31–C33	−0.2
C30–C29–C31–H34	−179.8	C29–C30–C32–C35	−0.5	C29–C30–C32–H36	179.3
C39–C30–C32–C35	179.1	C39–C30–C32–H36	−1.1	C29–C30–C39–C26	89.8
C29–C30–C39–H40	−31.7	C29–C30–C39–H41	−148.6	C32–C30–C39–C26	−89.7
C32–C30–C39–H40	148.7	C32–C30–C39–H41	31.9	C29–C31–C33–C35	−0.1
C29–C31–C33–H37	−179.8	H34–C31–C33–C35	179.5	H34–C31–C33–H37	−0.2
C30–C32–C35–C33	0.2	C30–C32–C35–H38	179.8	H36–C32–C35–C33	−179.6
H36–C32–C35–H38	−0.0	C31–C33–C35–C32	0.1	C31–C33–C35–H38	−179.5
H37–C33–C35–C32	179.8	H37–C33–C35–H38	0.2		

treating phenylaceticacid with thionylchloride. The compound was prepared as a new product. The structure of title compound was supported by spectral data. The ^{1}H NMR, mass spectra and elemental analysis results are in agreement with the proposed structure.

4.2. Antimicrobialactivities of the NBBPA

The newly synthesized was evaluated for their antibacterial activity against *S. aureus*, *E. faecalis* as Gram-positive, *E. coli, P. aeruginosa* as Gram-negative bacteria and their drug-resistant clinical isolate. All the microbiological result were shown in Table 1. According to antibacterial results NBBPA showed moderate activity against the tested microorganisms. The compound indicated more effect against drug-resistant *S. aureus* (64 μg/ml) and *E. coli* (128 μg/ml) than standard drug Gentamycin (128 μg/ml, 256 μg/ml, respectively). Moreover, this molecule found to be more active against *E. Faecalis* than tested the other microorganisms.

4.3. Computational and spectral studies

The mono-, tri-, 1,2-substituted phenyl rings and benzoxazole ring are designated as PhI, PhII, PhIII and PhIV in the following discussions.

4.3.1. Geometrical parameters

The C–C bond lengths in the phenyl ring lie in the range 1.3978–1.4055 Å for PhI phenyl ring, 1.3830–1.4168 Å for PhII phenyl ring and 1.3889–1.4145 Å for PhIII phenyl ring and for benzene the C–C bond length is 1.3993 Å [45]. The C–N bond lengths of the NBBPA, C_3–N_{24} = 1.4198 Å, C_5–N_{10} = 1.4103 Å and C_{26}–N_{24} = 1.3708 Å are less than the normal C–N bond (1.48 Å) shows some resonance in this section of the molecule [46]. The bond lengths, C_6–O_{22} = 1.3988 Å, C_{11}–O_{22} = 1.4273 Å and C_{11}=N_{10} = 1.3080 Å are in agreement with that of similar derivative [47]. The bond length C_{26}=O_{27} = 1.2509 Å is in agreement with the reported values [48]. In the present case, the C–Br bond length is 1.9469 Å which is in agreement with literature [49]. At C_{13} position, the bond angles are,C_{12}–C_{13}–C_{15} = 120.7°, C_{12}–C_{13}–Br_{23} = 123.7° and C_{15}–C_{13}–Br_{23} = 115.6° and this asymmetry shows the repulsion between bromine and benzoxazle ring. Similarly at C_{12} and C_{11} positions, the angles, C_{13}–C_{12}–C_{14} = 117.4°, C_{13}–C_{12}–C_{11} = 125.2°, C_{14}–C_{12}–C_{11} = 117.4° and N_{10}–C_{11}–C_{12} = 131.5°, N_{10}–C_{11}–O_{22} = 113.0°, C_{12}–C_{11}–O_{22} = 115.5° which shows the interaction between O_{22} and H_{17} atoms. The interaction between NH and neighbouring units is revealed by the bond angles around C_{26} and N_{24} which are respectively, C_{39}–C_{26}–N_{24} = 116.4°, C_{39}–C_{26}–O_{27} = 119.5°, N_{24}–C_{26}–O_{27} = 124.1° and $C2_6$–N_{24}–C_3 = 129.3°, C_{26}–N_{24}–H_{25} = 115.6°, C_3–N_{24}–H_{25} = 115.1°.

4.3.2. IR and Raman spectra

The observed IR, Raman bands are vibratioal assignments together with calculated scaled wavenumbers are given in Table 3.

The C=O stretching vibration is observed in the range 1800–1550 cm^{-1} [50], and for NBBPA the band observed at 1670 cm^{-1} experimentally is assigned as the C=O stretching mode which agrees with the computed value at 1673 cm^{-1} with a PED of 73% and high IR intensity of 398.27 and Raman activity of 59.03. In substituted benzenes, stretching vibrations of C–Br is expected in the range 635 ± 85 cm^{-1} [51] and for the NBBPA, this vibration is assigned at 687 cm^{-1} theoretically with PED 32% and this is in agreement with the reported values [49]. According to literature [52] the C=N stretching modes are expected in the region 1650–1500 cm^{-1} and for the NBBPA, this mode is assigned at 1511 cm^{-1} theoretically with a PED of 39% while the reported values are at 1520 cm^{-1} [53] and at 1536 cm^{-1} [54]. In the present casae, the C–N stretching modes are assigned at 1190, 1098 cm^{-1} (IR), 1192 cm^{-1} (Raman) and at 1222, 1188, 1100 cm^{-1} theoretically with PED contribution 34, 35, 40% as expected [52,55]. The C–O–C stretching modes of the title compound are assigned at 1137 and 956 cm^{-1} theoretically with PEDs 35 and 40%, with low IR intensities and the reported the C–O–C stretching modes are 1191, 1187, 988 and 993 cm^{-1} [53,56].

The N–H modes are normally expected in the regions, 3400 ± 40 cm^{-1} (stretching mode), 1510–1500, 1400–1300, 740–730 cm^{-1} (deformation modes) according to literature [50,51]. For NBBPA, the PED analysis gives the NH modes at 3450, 1524, 1262, 671 cm^{-1} theoretically with 99% PED for stretching mode, 45–37% PEDs for deformation modes and the deformation modes 1524 and 1262 cm^{-1} possess high Raman activity. Experimentally bands are observed at 3455, 3262, 1527, 1260, 670 cm^{-1} in the IR spectrum and at 1526 cm^{-1} in the Raman spectrum. The splitting in the IR spectrum and red shift from the computed value of the NH stretching vibration indicates the weakening of the NH bond as reported in literature [57].

Normally the CH_2 vibrational modes appear in the ranges, 2950–2850 cm^{-1} (stretching), 1470–900 cm^{-1} (deformations modes) [51,52,55] and the bands at 2936, 1422, 1165 cm^{-1} (IR), 2975, 2936, 1423, 1166 cm^{-1} (Raman) and 2969, 2934, 1425, 1285, 1167, 900 cm^{-1} (DFT) are assigned as the stretching and deformation modes of the CH_2 group of NBBPA.

The phenyl ring CH stretching modes are assigned at 3033 cm^{-1} (IR), 3071, 3050, 3020 cm^{-1} (Raman) for PhI and 3082, 3065 cm^{-1} (IR) for PhIII rings. The DFT calculations give these modes in the ranges, 3068–3036, 3118–3058 and 3094–3052 cm^{-1} for PhI, PhII and PhIII rings, respectively as expected [51]. The phenyl ring stretching modes are assigned at 1470, 1320 cm^{-1} (IR), 1588 cm^{-1} (Raman), 1585–1317 cm^{-1} (DFT) for PhI, 1577, 1541, 1391 cm^{-1} (IR), 1543, 1310 cm^{-1} (Raman), 1579–1309 cm^{-1} (DFT) for PhII and 1447 cm^{-1} (IR), 1605, 1567 cm^{-1} (Raman), 1597–1275 cm^{-1} (DFT) for PhIII rings which are in agreement with literature [51]. All the phenyl ring stretching modes possess a PED contribution equal or greater than 40%. In the case of tri-substituted phenyl rings with mixed substituents, the ring breathing mode is expected between 600 and 750 cm^{-1} [51,58] and in the present case the mode at 749 cm^{-1} (DFT) is assigned as the ring breathing mode of the tri-substituted benzene and the reported values are at 764 cm^{-1} (IR), 766 cm^{-1} (Raman) and at769 cm^{-1} (DFT) [59]. The ring breathing mode at 749 cm^{-1} has a PED of 50% with a high IR intensity and low Raman activity. For the NBBPA compound, the DFT calculations give the ring breathing mode of ortho substituted phenyl ring at 1111 cm^{-1} with a PED of 46% which is in agreement with literature [58] and the reported value is at 1087 cm^{-1} [60]. The band at 978 cm^{-1} with a PED of 40% is assigned as the ring breathing mode of the mono substituted phenyl ring of the NBBPA compound as expected [51,58]. Both the above two ring breathing modes have low IR intensities and experimentally no bands are seen in the IR spectrum. The in-plane CH bending modes of the phenyl rings are observed at 1282, 1070, 1017 cm^{-1} (IR), 1283, 1018 cm^{-1} (Raman) for PhI, 1129 cm^{-1} (IR), 1128 cm^{-1} (Raman) for PhII and at 1044 cm^{-1} (IR), 1246, 1045 cm^{-1} (Raman) for PhIII. The corresponding theoretical CH deformation modes of the phenyl rings are in the ranges, 1281–1013 cm^{-1} for PhI, 1235–1126 cm^{-1} for PhII and 1243–1043 cm^{-1} for PhIII [51]. The out-of-plane CH deformation modes of the phenyl rings are assigned at 968, 910, 725 cm^{-1} in the IR spectrum, 971, 726 cm^{-1}in the Raman spectrum for PhI, 951, 851, 824 cm^{-1} in the IR spectrum, 846 cm^{-1} in the Raman spectrum for PhII and no bands are seen experimentally for PhIII. The PED analysis gives these modes in the ranges, 969–726 cm^{-1} for PhI, 951–826 cm^{-1} for PhII and 960–741 cm^{-1} for PhIII rings,

Table 3
Calculated (scaled) wavenumbers, observed IR, Raman bands and vibrational assignments of *N*-[2-(2-bromophenyl)-1,3-benzoxazol-5-yl]-2-phenylacetamide.

B3LYP/6-311++G (5D, 7F)			IR	Raman	Assignments[a]
υ(cm^{-1})	IRI	RA	υ(cm^{-1})	υ(cm^{-1})	–
3450	85.42	322.96	3455, 3226	–	υNH(99)
3118	18.71	82.17	–	–	υCHII(96)
3094	1.99	94.67	–	–	υCHIII(97)
3081	4.45	190.46	3082	–	υCHIII(95)
3076	3.04	115.34	–	–	υCHII(96)
3068	11.19	282.61	–	3071	υCHI(93)
3066	11.71	226.15	3065	–	υCHIII(95)
3058	6.44	48.33	–	–	υCHII(99)
3057	21.11	43.31	–	–	υCHI(100)
3052	1.26	58.43	–	–	υCHIII(93)
3049	3.90	114.49	–	3050	υCHI(99)
3037	2.48	76.34	–	–	υCHI(99)
3036	5.57	14.31	3033	3020	υCHI(99)
2969	2.99	72.03	–	2975	υCH_2(99)
2934	11.05	237.43	2936	2936	υCH_2(99)
1673	398.27	59.93	1670	1670	υC═O (73)
1597	32.48	404.23	–	1605	δNH(18), υC═O(12), υPhIII(47)
1585	7.60	706.00	–	1588	υPhI(45), υPhII(18)
1579	6.91	49.75	1577	–	υC═O(21), υPhII(46), υPhI(12)
1566	7.58	1062.04	–	1567	υPhIII(51), δCHIII(23)
1558	0.97	8.00	–	–	υPhI(66), δCHI(21)
1539	35.14	450.64	1541	1543	υPhII(58), δCHIII(21)
1524	3.23	2622.68	1527	1526	δNH(44), υC═N(17)
1511	592.34	145.75	–	–	υC═N(39), δNH(12)
1467	11.15	2.32	1470	–	δCHI(14), υPhI(50)
1443	51.14	31.39	1447	–	δCHIII(13), υPhIII(49)
1440	49.03	88.51	–	–	υPhII(46), δCH_2(15), δCHII(13)
1425	5.96	0.85	1422	1423	δCH_2(77)
1409	0.45	41.06	–	–	δCHI(24), υPhI(42)
1399	17.82	10.57	–	–	δCHIII(23), υPhIII(40)
1396	139.44	232.47	1391	–	υPhII(48), δCHII(18)
1317	196.56	501.12	1320	–	υPhI(65), δCHII(10)
1309	0.36	0.16	–	1310	υPhII(50), υCN(15)
1285	0.01	1.91	–	–	δCH_2(56), δCHI(20)
1281	5.76	314.97	1282	1283	δCHI(56), υCN(17)
1275	1.60	24.13	–	–	υPhIII(77), δCHI(10)
1262	32.38	694.12	1260	–	δNH(45), υCN(14)
1243	14.04	5.13	–	1246	δCHIII(62), υCN(25)
1235	41.57	430.58	–	–	υPhII(18), δCHII(43), υCN(15)
1222	9.38	570.34	–	–	υCN(34), υCC(13), υPhIII(22)
1188	87.80	18.62	1190	1192	υCC(33), υCN(35)
1175	1.41	41.66	–	–	υCC(31), υCN(18), δCH_2(20)
1167	109.86	251.05	1165	1166	δCH_2(62), υPhI(18)
1159	0.15	2.62	–	–	δCHI(72), υPhI(20)
1158	0.24	3.30	–	–	δCHIII(83), υPhII(11)

(*continued on next page*)

Table 3 (*continued*)

B3LYP/6-311++G (5D, 7F)			IR	Raman	Assignments[a]
υ(cm^{-1})	IRI	RA	υ(cm^{-1})	υ(cm^{-1})	–
1146	3.66	43.49	–	–	δCHI(67), υPhI(16)
1137	0.01	2.53	–	–	υCO(35), δCHII(33)
1126	4.91	131.33	1129	1128	δCHII(46), υCN(11), υPhII(17)
1111	10.42	5.20	–	–	δCHIII(41), υPhIII(46)
1100	6.88	32.78	1098	–	υCN(40), δCHII(21)
1060	6.85	0.13	1070	–	υPhI(12), δCHI(45)
1043	3.21	5.56	1044	1045	υCC(17), δPhIII(18), δCHIII(43)
1013	27.21	104.08	1017	1018	δCHI(52), υPhI(16)
1010	3.86	13.75	–	1010	δCHIII(39), τPhIII(18)
990	85.01	79.26	–	–	υPhIII(46), υPhI(16), υCBr(11)
978	0.30	43.70	–	–	δPhI(13), υPhI(40)
969	0.13	0.31	968	971	γCHI(74), τPhI(14)
960	0.01	0.60	–	–	γCHIII(94)
956	7.20	16.03	–	–	δPhIII(22), υCO(40), δPhIV(27)
951	0.01	0.01	951	–	γCHII(88)
938	0.34	0.39	–	–	γCHI(92)
935	1.52	0.06	932	933	υCC(16), υPhII(21), δPhII(19)
904	7.89	151.17	910	–	γCHI(77)
900	6.28	13.71	–	–	δCH_2(68), γC═O(15)
898	3.91	14.55	–	–	γCHIII(70), τPhIII(10)
893	0.88	0.57	–	–	δCN(19), δPhII(12), υCC(31), υPhII(10)
847	0.01	0.10	851	846	γCHII(78), τPhII(10)
836	28.34	0.03	–	–	γCHIII(68), δPhIV(26)
828	11.60	17.79	–	–	γCHI(98)
826	0.69	0.29	824	–	γCHII(90)
808	23.75	2.13	–	–	δCH_2(13), δCN(11), γCHI(11), υPhI(10)
806	27.47	0.06	804	807	υCO(14), δCN(20), δPhII(32)
789	2.16	10.52	–	–	τPhIII(33), γCC(31), γCHIII(29)
749	33.83	2.83	748	–	υPhII(50), δCN(10)
741	15.02	0.81	–	–	γCHIII(72), τPhIII(17)
726	2.46	0.14	725	726	τPhI(22), γCHI(47), γCC(10)
710	32.41	1.42	–	–	δPhIII(48), υCBr(10), δCH_2(17)
697	11.38	5.79	695	–	τPhI(56), γCHI(37)
687	53.20	0.75	–	–	υCBr(32), τPhII(13), τPhIV(18), γCN(11)
671	2.64	0.26	670	–	γNH(37), τPhIV(20), γCC(11), τPhIII(10), τCN(16)
668	4.26	3.35	670	–	τPhIV(32), τPhIII(18), γCC(18), γNH(14)
633	5.73	12.01	633	640	δPhIV(20), δPhI(19), δPhII(14)
617	4.39	0.58	616	–	δPhIII(71)
611	0.70	3.57	–	612	δPhI(87)
605	7.87	0.03	–	–	δPhI(28), τPhI(11), δCH_2(23)
602	4.72	0.97	–	–	γCN(23), τPhII(23), τPhIV(12), τPhI(14)
582	11.10	15.88	–	–	δPhIII(40),

Table 3 (*continued*)

B3LYP/6-311++G (5D, 7F)			IR	Raman	Assignments[a]
υ(cm^{-1})	IRI	RA	υ(cm^{-1})	υ(cm^{-1})	–
					δPhIV(12)
543	21.96	0.47	–	–	γC═O(60), δCH_2(13)
536	2.57	3.57	537	–	δCC(37), δPhII(19)
509	37.75	3.92	512	514	τPhIII(56), γCC(11), τPhIV(11)
500	0.01	0.11	–	–	τPhI(23), γCC(17), δPhII(23)
439	6.40	0.10	441	–	τPhIII(54), γCBr(22)
429	1.06	1.12	429	–	τPhI(37), γCC(11), δC═O(10)
419	3.21	–	417	417	τPhII(61), τPhIII(10)
402	8.33	1.46	402	–	τPhI(85)
398	0.02	0.01	–	–	δCN(26), δCC(19), δPhII(16)
369	0.01	0.36	–	–	τPhIV(39), τPhII(13), τPhIII(10), γCN(12)
360	9.14	6.42	–	355	δCBr(26), δC═O(19), δCN(22)
328	0.24	4.28	–	–	δCBr(15), τPhI(14), δCN(16), δCH_2(19)
314	0.61	0.23	–	–	δCC(68), δCH_2(10)
295	1.97	8.07	–	–	τPhIII(27), τPhII(28), τPhIV(13)
294	0.15	0.87	–	–	δCBr(30), δCN(22)
228	4.10	1.40	–	–	τPhI(24), δCN(18), δCBr(10), δPhIII(11)
217	0.11	2.20	–	–	τPhII(49), τPhIV(22)
200	3.38	1.72	–	–	δCBr(20), δCN(18), δCC(10)
185	0.14	0.69	–	–	τPhII(14), τPhIII(13), γCBr(12), τPhIV(11), τCN(10), γCC(14)
164	0.39	2.85	–	162	δCBr(18), τPhI(16), δPhII(28)
118	2.15	2.00	–	124	τPhIII(50), τPhIV(10), γCBr(10)
117	0.47	2.42	–	–	δCBr(15), δCN(27), γCC(13), δCC(13)
72	0.01	1.32	–	–	τCN(18), γCC(25), γNH(18), τCC(11)
61	0.18	1.31	–	–	δCC(43), γCC(16), δCH_2(15)
51	6.59	0.04	–	–	τNH(26), τCC(21), τCH_2(16), τCN(19)
35	1.09	4.85	–	–	τCC(51), τNH(17)
30	0.32	2.37	–	–	τCH_2(36), τCC(22), τNH(20)
29	0.67	5.08	–	–	δCH_2(20), γCC(16), δCN(37)
17	0.04	2.63	–	–	τCH_2(42), τCN(13), τCC(23)
6	0.71	2.10	–	–	τCC(61), τCH_2(31), τNH(10)

[a] υ-stretching; δ-in-plane deformation; γ-out-of-plane deformation; τ-torsion; PhI-mono substituted phenyl ring; PhII-tri-substituted phenyl ring; PhIII-di-substituted phenyl ring; PhIV-benzoxazole ring; potential energy distribution (%) is given in brackets in the assignment column.

respectively [51].

4.3.3. NMR spectra

The absolute isotropic chemical shielding of the NBBPA molecule was calculated using B3LYP/GIAO model and the results have been shown in Table 4. The ^{1}H NMR experimental values are: ^{1}H NMR (ppm): 3.60 (CH_2, 2H, s); 7.08–7.78 (phenyl protons, 9H, m); 7.60–7.64 (C1 of benzoxazole, 1H, d, $J_{7,6}$: 9.2 Hz), 7.90–7.95 (C2 of benzoxazole, 1H, dd, $J_{6,4}$: 1.6 Hz, $J_{6,7}$:7.8 Hz), 8.06–8.09 (C4 of benzoxazole, 1H, d, $J_{4,6}$: 2.4 Hz), 10.30 (NH, 1H, s). The protons of the phenyl rings, PhI, PhII and PhIII resonate in the ranges, 7.7804–7.9211, 6.7663–9.39 and 7.6219–8.8452 ppm theoretically. The chemical shift of hydrogen atom associated with the NH group is 6.2093 ppm and for the hydrogen atoms of the CH_2 groups is 4.124 and 4.1239 ppm. The predicted shifts of carbon atoms are 127.7619–134.8546 ppm for PhI, 108.7313–145.5238 ppm for PhII

Table 4
Calculated NMR parameters (with respect to TMS).

Protons	σ_{TMS}	σ_{calc}	$\delta_{calc} = \sigma_{TMS} - \sigma_{calc}$
H7	32.7711	25.0983	7.6728
H8	32.7711	23.3811	9.3900
H9	32.7711	26.0048	6.7663
H17	32.7711	23.9259	8.8452
H19	32.7711	24.8866	7.8845
H20	32.7711	25.0698	7.7013
H21	32.7711	25.1492	7.6219
H25	32.7711	26.5618	6.2093
H28	32.7711	24.9907	7.7804
H34	32.7711	24.85	7.9211
H36	32.7711	24.9906	7.7805
H37	32.7711	24.9097	7.8614
H38	32.7711	24.8501	7.9210
H40	32.7711	28.6471	4.1240
H41	32.7711	28.6472	4.1239
Carbon atoms			
C1	196.852	85.7999	111.0521
C2	196.852	79.2258	117.6262
C3	196.852	59.3433	137.5087
C4	196.852	88.1207	108.7313
C5	196.852	53.9699	142.8821
C6	196.852	51.3282	145.5238
C11	196.852	37.2263	159.6257
C12	196.852	67.762	129.0900
C13	196.852	52.7907	144.0613
C14	196.852	64.9735	131.8785
C15	196.852	60.8552	135.9968
C16	196.852	70.5372	126.3148
C18	196.852	67.3127	129.5393
C26	196.852	33.7502	163.1018
C29	196.852	66.3824	130.4696
C30	196.852	61.9974	134.8546
C31	196.852	67.7182	129.1338
C32	196.852	66.3833	130.4687
C33	196.852	69.0901	127.7619
C35	196.852	67.718	129.1340
C39	196.852	144.4808	52.37120

and 126.3148–144.0613 ppm for PhIII rings. For the carbon atoms, C39, C26 and C11, the predicted shifts are 52.3712, 163.1018 and 159.6257 ppm respectively.

4.3.4. Nonlinear optical studies

The interaction of electromagnetic fields in various media to produce new physical properties, produce nonlinear optical effects [61]. For the title compound, the polarizability, first hyperpolarizability and second hyperpolarizability are respectively, 4.4539×10^{-23}, 6.8293×10^{-30} and -36.898×10^{-37} esu and these values of the investigated molecule clearly reveal that they have nonlinear optical behavior with non-zero values. The reported values of the first hyperpolarizability of similar derivates are 2.66×10^{-30} esu [62] and 1.37×10^{-30} esu [47] and the first hyperpolarizability of the title compound is 52.53 times that of the standard NLO material urea [63]. The C–N bond lengths in the title compound are intermediate between a single and double bond which produces an extended π-electron delocalization over the molecular system [64]which is responsible for the nonlinearity of the system.

4.3.5. Frontier molecular orbitals

The site selectivity and chemical reactivity such as the electronic chemical potential, μ, hardness, η, global electrophilicity, μ, can be defined successfully by DFT methods [65,66]. The HOMO-LUMO plots are shown in Fig. 4 and HOMO is localized over the whole molecule except the mono-substituted phenyl ring and CH_2 group while the LUMO is over the whole molecule except over the mono-substituted phenyl ring, CH_2 and acetamide group. For the NBBPA

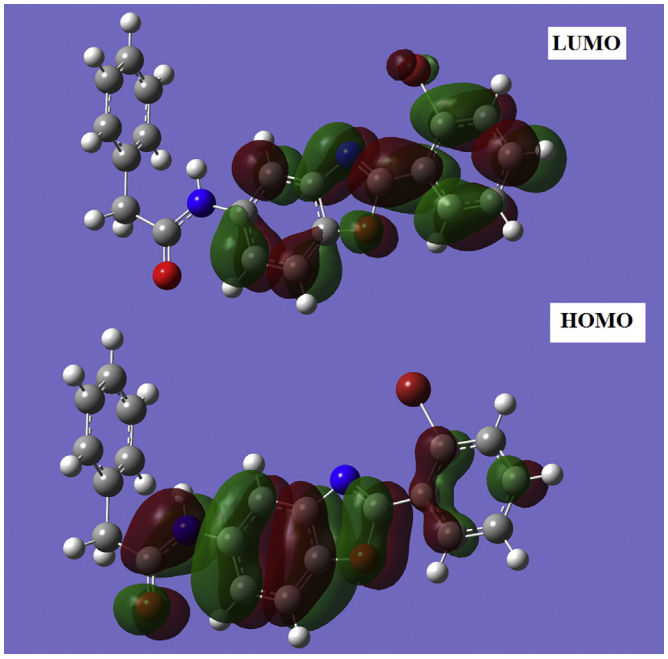

Fig. 4. HOMO-LUMO plots of *N*-[2-(2-bromophenyl)-1,3-benzoxazol-5-yl]-2-phenyl acetamide.

compound, $E_{HOMO} = -8.131$ eV and $E_{LUMO} = -5.318$ eV and the energy gap = 2.813 eV. According to the literature data [67–71], the chemical potential $\mu = -(I + A)/2$ where $I = -E_{HOMO}$ and $A = -E_{LUMO}$ are ionization potential and electron affinity; harness, $\eta = (I\text{-}A)/2$ and electrophilicity index, $\omega = \mu^2/2\eta$. The different descriptors are: $\mu = 6.7245$, $\eta = 1.4065$ and $\omega = 16.075$.

4.3.6. Molecular electrostatic potential

Using the molecular electrostatic potential map the charge distribution of a molecule can be pictured which is important because, these values determine how molecules interact with one another as they point out the reactive sites in the molecule. In the MEP plot (Fig. 5) blue regions are the stronger positive regions and red regions are the lower electrostatic potential regions. From the MEP plot it is very clear that carbonyl and NH groups are the lower electrostatic potential sites favorable of electrophilic reactive regions and other parts of the NBBPA molecule are favorable for nucleophilic reactive regions.

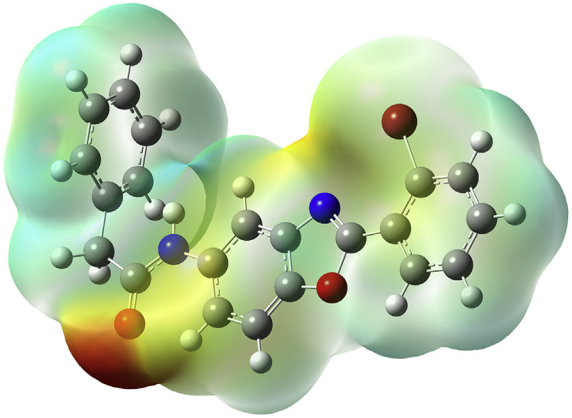

Fig. 5. MEP plot of *N*-[2-(2-bromophenyl)-1,3-benzoxazol-5-yl]-2-phenyl acetamide.

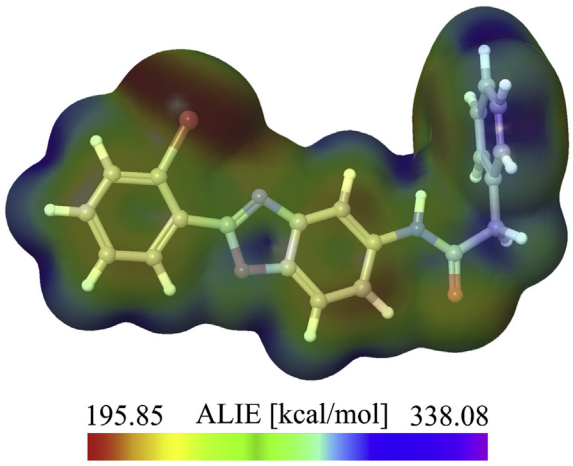

Fig. 6. ALIE surface of *N*-[2-(2-bromophenyl)-1,3-benzoxazol-5-yl]-2-phenyl acetamide molecule.

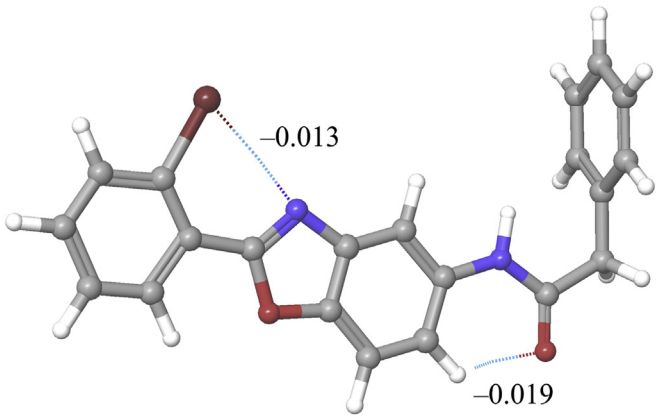

Fig. 7. Intramolecular noncovalent interactions and their strengths (in electron/bohr^3) of *N*-[2-(2-bromophenyl)-1,3-benzoxazol-5-yl]-2-phenyl acetamide molecule.

4.3.7. ALIE surface, Fukui functions and non-covalent interactions

In order to investigate reactive properties of organic molecules Sjoberg et al. have introduced average local ionization energy (ALIE) [72,73]. The definition of this quantum-molecular descriptor is based on sum of orbital energies weighted by the orbital densities according to the following equation:

$$I(r) = \sum_i \frac{\rho_i(\vec{r})|\varepsilon_i|}{\rho(\vec{r})}. \quad (1)$$

where $\rho_i(\vec{r})$ denotes electronic density of the i-th molecular orbital at the point $\vec{r}$, ε_i denotes orbital energy, while $\rho(\vec{r})$ denotes total electronic density function. ALIE indicates the energy necessary for the removal of electron from the certain point around the molecules. This quantity can be represented as maximal and minimal value for each atom, or its values can be mapped to the electron density surface. The later mentioned method, applied in this work, enables visualization of molecule locations prone to the electrophilic attacks, Fig. 6.

Inspection of ALIE surface presented in Fig. 6 indicates that there are two specific molecule sites prone to electrophilic attacks (designated by the red color). In this regard near vicinity of bromine atom Br23 and near vicinity of central benzene ring are characterized by ALIE values which indicate that here electrons are least tightly bound and therefore the most easily removed. These molecule sites are characterized by the ALIE value of around 196 kcal/mol. On the other side the highest ALIE values are around 338 kcal/mol and are localized in the near vicinities of hydrogen atoms.

Charge density analysis in the case of NBBPA molecule revealed the existence of two intramolecular noncovalent interactions, Fig. 7. These noncovalent interactions are located between bromine and nitrogen atoms (Br23—N10) and between oxygen and hydrogen atoms (O27—H8). Both of these noncovalent interactions are strong, with the one between oxygen and hydrogen atom being significantly stronger.

Further investigation of local reactivity properties encompassed the calculations of Fukui functions, which are calculated in Jaguar program by finite difference approach according to the following equations:

$$f^+ = \frac{\left(\rho^{N+\delta}(r) - \rho^N(r)\right)}{\delta}, \quad (2)$$

$$f^- = \frac{\left(\rho^{N-\delta}(r) - \rho^N(r)\right)}{\delta}. \quad (3)$$

In equations (2) and (3), N stands for the number of electrons in reference state of the molecule, while δ stands for the fraction of electron which default value is set to be 0.01 [74]. Mapping of the Fukui functions to the electron density surface enables visualization of molecule sites where electron density increase or decrease as a consequence of charge addition or removal, Fig. 8. In the case of Fukui f^+ function it is necessary to track the positive color (purple color in Fig. 8a), which indicates the molecule sites where electron density increased after the addition of charge. In this regard it can be seen that after charge addition electron density increased in the near vicinity of atoms of benzene ring with bromine atom and in the near vicinity of carbon atom C11, indicating that these molecule sites act as electrophiles. In the case of Fukui f^- function it is necessary to track the negative color (red color in Fig. 8b), which shows the molecule sites where electron density decreased after the removal of charge. It can be seen in Fig. 8b that electron density decreased in the near vicinity of terminal benzene ring, showing that this part of the molecule could act as nucleophile.

4.3.8. Natural bond orbital analysis

The natural bond orbitals (NBO) calculations were performed using NBO 3.1 program [75] as implemented in the Gaussian09 package at the DFT/B3LYP level and the results are tabulated in Tables 5 and 6. The strong inter-molecular hyper-conjugative interaction are: C_{11}—C_{12} from N_{10} of $n_1(N_{10}) \rightarrow \sigma^*(C_{11}$—$C_{12})$, N_{10}—C_{11} from O_{22} of $n_2(O_{22}) \rightarrow \pi^*(N_{10}$—$C_{11})$, C_{12}—C_{13} from Br_{23} of $n_3(Br_{23}) \rightarrow \pi^*(C_{12}$—$C_{13})$, C_{26}—O_{27} from N_{24} of $n_1(N_{24}) \rightarrow \pi^*(C_{26}$—$O_{27})$, N_{24}—C_{26} from O_{27} of $n_2(O_{27}) \rightarrow \sigma^*(N_{24}$—$C_{26})$ having electron densities, 0.03329, 0.30325, 0.44545, 0.29909, 0.07226e and stabilization energies of 14.28, 28.72, 10.08, 64.93, 23.26 kJ/mol. The natural hybrid orbital with low occupation numbers, higher energies and considerable p-character are: $n_2(O_{22})$, $n_3(Br_{23})$, $n_2(O_{27})$ with energies, −0.3278, −0.28331, −0.23752a.u and p-characters, 100.0, 100.0, 99.95% and low occupation numbers, 1.74929, 1.92825, 1.86624 while the orbital with high occupation number, lower energies are: $n_1(O_{22})$, $n_2(Br_{23})$, $n_1(O_{27})$ with energies, −0.60252, −0.28482, −0.67917a.u. and p-characters, 58.72, 99.34, 38.97% and occupation numbers, 1.97241, 1.97414,

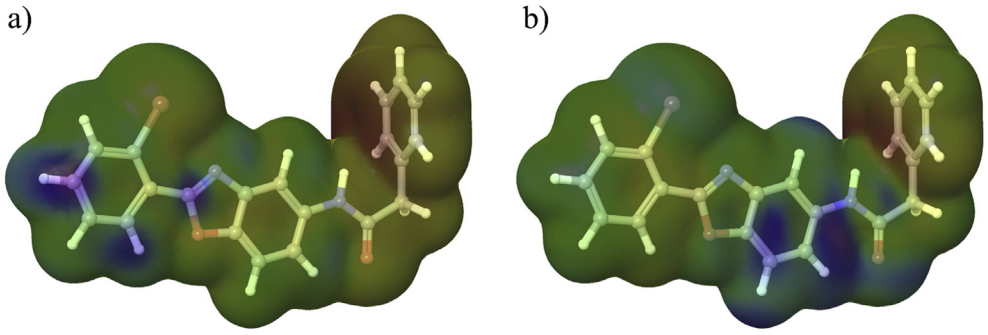

Fig. 8. Fukui functions a) f^{+} and b) f^{-} of the *N*-[2-(2-bromophenyl)-1,3-benzoxazol-5-yl]-2-phenyl acetamide molecule.

Table 5
Second-order perturbation theory analysis of Fock matrix in NBO basis corresponding to the intra-molecular bonds of the title compound.

Donor(i)	Type	ED/e	Acceptor(j)	Type	ED/e	E(2)[a]	E(j)-E(i)[b]	F(i,j)[c]
C3–C4	π	1.68597	C1–C2	π*	0.33296	17.93	0.29	0.065
C3–C4	π	1.68597	C5–C6	π*	0.46084	20.70	0.28	0.071
C5–C6	π	1.60101	C1–C2	π*	0.33296	19.33	0.29	0.068
C5–C6	π	1.60101	C3–C4	π*	0.38314	18.67	0.28	0.065
C5–C6	π	1.60101	N10–C11	π*	0.30325	10.97	0.26	0.049
N10–C11	π	1.86715	C5–C6	π*	0.46084	14.53	0.34	0.069
LP N10	σ	1.90927	C11–C12	σ*	0.03329	14.28	0.64	0.086
LP O22	π	1.74929	C5–C6	π*	0.46084	21.58	0.35	0.082
LP O22	π	1.74929	N10–C11	π*	0.30325	28.72	0.33	0.089
LP Br23	n	1.92825	C12–C13	π*	0.44545	10.08	0.29	0.053
LP N24	σ	1.65272	C3–C4	π*	0.38314	31.93	0.29	0.086
LP N24	σ	1.65272	C26–O27	π*	0.29909	64.93	0.27	0.119
LP O27	π	1.86624	N24–C26	σ*	0.07226	23.26	0.70	0.116
LP O27	π	1.86624	C26–C39	σ*	0.06509	18.66	0.60	0.096

[a] E(2) means energy of hyper-conjugative interactions (stabilization energy kJ/mol).
[b] Energy difference between donor and acceptor i and j NBO orbitals.
[c] F(i,j) is the Fock matrix element between i and j NBO orbitals.

Table 6
NBO results showing the formation of Lewis and non Lewis orbitals.

Bond (A-B)	ED/e[a]	EDA%	EDB%	NBO	s%	p%
πC3-C4	1.68597	49.21	50.79	0.7015 ($sp^{1.00}$)C	0.00	100.00
_	−0.25489	–	–	+0.7126 ($sp^{1.00}$)C	0.00	100.00
πC5-C6	1.60101	49.78	50.22	0.7055 ($sp^{1.00}$)C	0.00	100.00
_	−0.25756	–	–	+0.7087 ($sp^{1.00}$)C	0.00	100.00
πN10-C11	1.86715	58.40	41.60	0.7642 ($sp^{1.00}$)N	0.00	100.00
_	−0.31882	–	–	+0.6450 ($sp^{1.00}$)C	0.00	100.00
n1 N10	1.90927	–	–	$sp^{2.02}$	33.07	66.93
_	−0.36852	–	–	–	–	–
n1 O22	1.97241	–	–	$sp^{1.43}$	41.18	58.72
_	−0.60252	–	–	–	–	–
n2 O22	1.74929	–	–	$sp^{1.00}$	0.00	100.00
_	−0.32784	–	–	–	–	–
n1 Br23	1.99512	–	–	$sp^{0.15}$	86.85	13.15
_	−0.93118	–	–	–	–	–
n2 Br23	1.97414	–	–	$sp^{99.99}$	0.66	99.34
_	−0.28482	–	–	–	–	–
n3 Br23	1.92825	–	–	$sp^{1.00}$	0.00	100.00
_	−0.28331	–	–	–	–	–
n1 N24	1.65272	–	–	$sp^{1.00}$	0.00	100.00
_	−0.26022	–	–	–	–	–
n1 O27	1.97473	–	–	$sp^{0.64}$	61.03	38.97
_	−0.67917	–	–	–	–	–
n2 O27	1.86624	–	–	$sp^{99.99}$	0.05	99.95
_	−0.23752	–	–	–	–	–

[a] ED/e is expressed in a.u.

1.97473.

4.3.9. Reactive and degradation properties based on autoxidation and hydrolysis

Computational analysis of molecules based on the combination of DFT calculations and MD simulations allows inexpensive initial prediction of degradation properties. In this regard it is useful to note that bond dissociation energy (BDE) for hydrogen abstraction indicate to what extent is some molecule prone to autoxidation mechanism, while BDE values for the rest of the single acyclic bonds can serve for the classification of bonds according to their strengths. These results are important for the rationalization and optimization of procedures related to forced degradation studies [76–79]. Analysis of BDEs for hydrogen abstraction can indicate whether some molecule is prone to autoxidation mechanism or not. According to the Wright et al. [80], for investigated pharmaceutical molecule can be concluded that it is vulnerable towards autoxidation mechanism if the BDE ranges from 70 to 85 kcal/mol. Gryn'ova et al. [81] agrees with this statement, but also states that in this regard C–H dissociation is questionable for the BDE values in the range between 85 and 90 kcal/mol, meaning that BDE values for hydrogen abstraction in this range could also be important for the autoxidation mechanism. When BDE values for hydrogen abstraction are lower than 70 kcal/mol, formed radicals are resistant for the O_2insertion [25,80–82] and these values are not suitable for autoxidation mechanism.

In Fig. 9 all BDE values have been provided. Values provided in red color corresponds to the BDE values for hydrogen abstraction, while values provided in blue corresponds to the BDE values for the

rest of the single acyclic bonds. Results presented in Fig. 9 indicate that NBBPAmolecule is very stable in open air and in the presence of oxygen since there are no BDE values for hydrogen abstraction in the range from 70 to 85 kcal/mol. The lowest BDE value for hydrogen abstraction is 91.53 kcal/mol, which is higher even than upper limit defined by Wright and Gryn'ova. On the other side the lowest BDE values for the rest of the single acyclic bonds have been calculated for bonds denoted with numbers 13 and 15, indicating that degradation could start by detaching of bromine atom or terminal benzene ring.

Comparison of atoms of NBBPAmolecule with regard to their interactions with water molecules have been performed by calculations of radial distribution functions (RDFs) after MD simulations. RDF, g(*r*), indicates the probability of finding a particle in the distance *r* from another particle [83]. RDFs that resemble the most important interactions with water molecules are presented in Fig. 10. According to the results presented in Fig. 10, six atoms of NBBPAmolecule have pronounced interactions with water. g(r) curves of carbon atoms C1, C4 and C26 are very similar in terms of profile and peak distance (around 3.5 Å), with atom C4 having somewhat lower maximal g(r) value comparing with C1 and C26. g(r) curve of bromine atom Br23 is also similar with carbons, but it's maximal g(r) value is the highest of all atoms with significant interactions with water molecules. However, the most important interactions with water molecules according to RDFs can be seen for oxygen atom O27 and hydrogen atom H25. The maximal g(r) value for O27 is located at distance of around 2.6 Å, while in the case of H25 maximal g(r) value is located at around 1.8 Å, indicating strong interactions with water in both cases.

4.3.10. Molecular docking studies

DNA gyrase basically consisted of two subunits (A and B) and functions by dimer form of these subunits. The ATP binding pocket, which is founded highly conserved between species is located in subunit B of DNA gyrase, and defined by N45, E49, D72, R75, I77, K102, V117, and T164 residues in *T. thermophilus* and *E. coli* DNA gyrase subunit B (GyrB). This region is thought to be a drug target for antibacterial agents [84–86]. High resolution crystal structure of DNA gyrase B form complex was downloaded from the protein data bank website (PDB ID: 1KIJ [87]. All molecular docking calculations were performed on Auto Dock Vina software [88]. Receptor was in dimer form so firstly one of the subunit B was

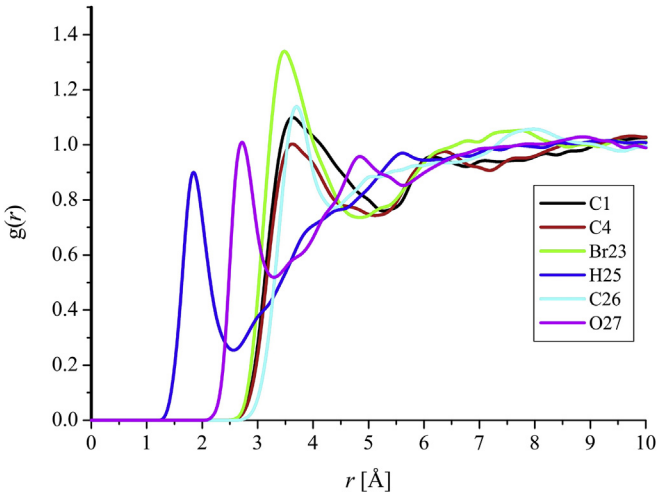

Fig. 10. RDFs of *N*-[2-(2-bromophenyl)-1,3-benzoxazol-5-yl]-2-phenyl acetamide's atoms with significant interactions with water molecules.

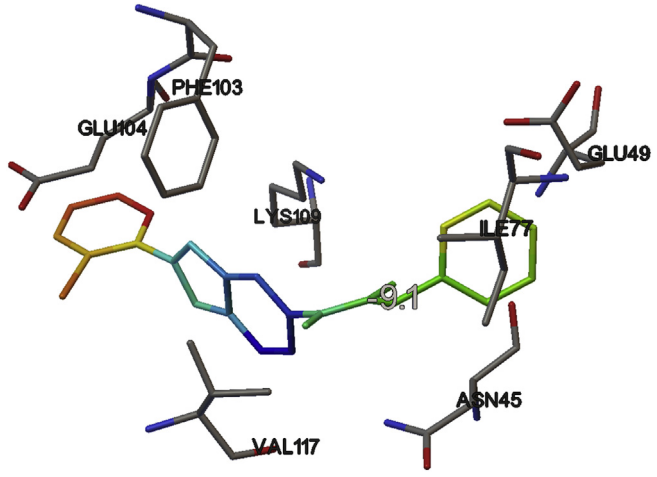

Fig. 11. Receptor ligand interactions which were determined by Autodock. The weak noncovalent interactions with N45, E49, I77, F103, E104, K109, V117 amino acid residues.

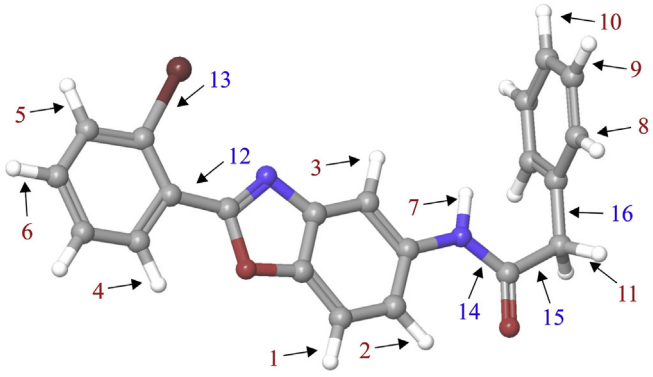

Bond	BDE [kcal/mol]
1	119.28
2	119.47
3	119.84
4	117.54
5	117.71
6	117.86
7	106.34
8	117.23
9	117.50
10	117.85
11	91.53
12	119.31
13	66.70
14	82.93
15	70.45
16	95.42

Fig. 9. BDEs of all single acyclic bonds of *N*-[2-(2-bromophenyl)-1,3-benzoxazol-5-yl]-2-phenyl acetamidemolecule

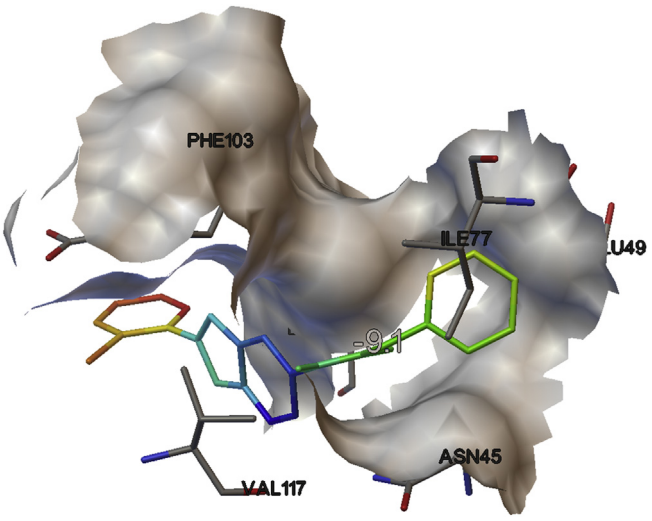

Fig. 12. Molecular surface model of Autodock analyzing.

removed and then the receptor was prepared by the cleaning of all heteroatom's (i.e., nonreceptor atoms such as water, ions, co-crystallized ligand, etc.). The Auto Dock Tools (ADT) graphical user interface was used to calculate Gasteiger charges and polar hydrogen's. Ligand and receptor input files were arranged in PDBQT format. The docking area was defined around the ATP binding site, which was determined in crystal structure, by a grid box of 40 Å × 40 Å × 40 Å using 0.375 Å grid point spacing in AutoGrid. The docking conformations of ligands in the binding sites of the receptor were searched with Lamarkian genetic Algorithm (LGA) in Autodock. The cocrystallized inhibitor was extracted from receptor and docked again for the affordance of the docking protocol. The docking protocol predicted the same conformation as was present in the crystal structure with RMSD value well within the reliable range of 2 Å [89]. Amongst the docked conformations, one which binded well the active site was analyzed for detailed interactions with ADT and Discover Studio Visualizer 3.5 software [90]. The ligand binds at the active site of the substrate (Figs. 11–13) by weak noncovalent interactions with N45, E49, I77, F103, E104, K109, V117 amino acid residues. Discover Studio Visualizer was also predicted electrostatic interactions with N45, D48, E104, K109, V117 and van der Waals interactions with E49, I77, F103, Q105, T166. E104 forms π–ς bond with benzene ring which attaches to bromine and K109 also forms π-cation bond with the other benzene rings of compound. The docked ligand title compound forms a stable complex with GyrB complex and gives a binding affinity (ΔG in kcal/mol) value of −9.1 (Table 7). These preliminary results suggest that the compound might exhibit inhibitory activity against GyrB complex.

5. Conclusion

Microbiological results against Gram-negative (*E. coli, P. aeruginosa*) and Gram-positive (*S. aureus, E. faecalis*) bacteria showed that *N*-[2-(2-bromophenyl)-1,3-benzoxazol-5-yl]-2-phenylacetamide compound exhibit higher activity against *E. coli* and *S. aureus*, with MIC values of 128 μg/ml and 64 μg/ml respectively, than the standard drug Gentamycin. Additionally, it was found that the activity against *E. faecalis* was more potent than to

Table 7
The binding affinity values of different poses of the title compound predicted by AutodockVina

Mode	Affinity (kcal/mol)	Distance from best mode (Å)	
–	–	RMSD l.b.	RMSD u.b.
1	−9.1	0.000	0.000
2	−8.4	1.661	2.464
3	−7.9	2.733	2.931
4	−7.8	6.935	10.325
5	−7.3	5.849	12.456
6	−6.9	5.934	9.303
7	−6.8	6.121	12.734

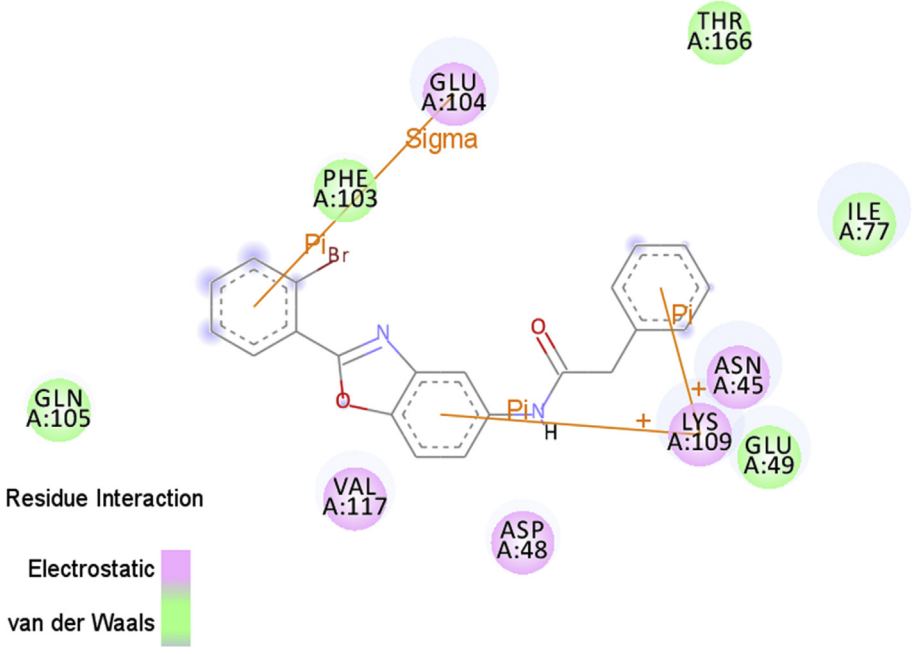

Fig. 13. Receptor ligand interactions which were determined by Discovery Studio Client 3.5. π–ς bond between benzene ring which bounds bromine and e104. K109 also forms π-cation bond with the other benzene rings of compound.

other tested microorganisms. The red shift and splitting of NH stretching mode shows the weakening of the NH bond, while the first hyperpolarizability of the title compound is 52.53 times that of the standard NLO material – urea. It was also concluded that C–N bond lengths an extended π-electron delocalization over the molecular system, which is responsible for the nonlinearity of the molecule. The carbonyl and NH groups are favorable sites for electrophilic attacks, while ALIE surface indicated the significance of bromine atom in terms of electrophilic attacks. HOMO is spread over the whole molecule, except the mono-substituted phenyl ring and CH_2 group, while LUMO is spread over the whole molecule, except over the mono-substituted phenyl ring, CH_2 and acetamide group. HOMO and LUMO visualization indicates charge transfer within the molecule. Fukui functions show that benzene ring with bromine atom and terminal benzenering could have significant importance with the addition and removal of charge. Analysis of electron density determined that there are two intramolecular noncovalent interactions. BDE values for hydrogen abstraction indicate high stability of the title molecule in the open air or in the presence of oxygen, while BDE values of the rest of the single acyclic bonds indicate that degradation could start with the detaching bromine atom. RDFs obtained after MD simulations indicate that there are six atoms of NBBPA molecule with significant interactions with water molecules among which the most important are hydrogen atom H25 and oxygen atom O27. The docked title compound forms a stable complex with GyrB complex and gives a binding affinity value of −9.1 kcal/mol and might exhibit inhibitory activity against GyrB complex. Obtained results concerning antimicrobial activity emphasize the potential of NBBPA molecule for further studies, while other results encompassed by this study provide important insights into the reactivity of the title compound.

Acknowledgments

Part of this work has been performed thanks to the support received from Schrödinger Inc. Part of this study was conducted within the projects supported by the Ministry of Education, Science and Technological Development of Serbia, grant numbers OI 171039 and TR 34019. Additionally, this study is supported by a grant (Project Number:16H0237002) from Scientific Research Projects Committee of Ankara University.

References

[1] I. Oren, O. Temiz, I. Yalcin, E. Sener, A. Akin, N. Ucarturk, Synthesis and microbiological activity of 5 (or 6)-methyl-2-substituted benzoxazole and benzimidazole derivatives, Arzneim. Forsch./Drug. Res. 47 (12) (1997) 1393–1397.
[2] I. Yalcin, I. Oren, E. Sener, A. Akin, N. Ucarturk, The synthesis and the structure-activity relationships of some substituted benzoxazoles, oxazolo(4,5-b)pyridines, benzothiazoles and benzimidazoles as antimicrobial agents, Eur. J. Med. Chem. 27 (1992) 401–406.
[3] I. Oren-Yildiz, I. Yalcin, E. Aki-Sener, N. Ucarturk, Synthesis and structure-activity relationships of new antimicrobial active multisubstituted benzazole derivatives, Eur. J. Med. Chem. 39 (2004) 291–298.
[4] O. Temiz-Arpaci, A. Ozdemir, I. Yalcın, I. Yıldız, E. Akı-Sener, N. Altanlar, Synthesis and antimicrobial activity of some 5-[2-(morpholin-4-yl)acetamido] and/or 5-[2-(4-substituted piperazin-1-yl)acetamido]-2-(p-substituted phenyl) benzoxazoles, Arch. Pharm. 338 (2005) 105–111.
[5] J. Vinsova, V. Horak, V. Buchta, J. Kaustova, Highly lipophilic benzoxazoles with potential antibacterial activity, Molecules 10 (2005) 783–793.
[6] A. Akbay, I. Oren, O. Temiz-Arpaci, E. Aki-Sener, I. Yalcin, Synthesis and HIV-1 reverse transcriptase inhibitor activity of some 2,5,6-substituted benzoxazole, benzimidazole, benzothiazole and oxazolo (4,5-b) pyridine derivatives, Arzneim. Forsch 53 (2003) 266–271.
[7] A. Pinar, P. Yurdakul, I. Yildiz-Oren, O. Temiz-Arpaci, N.L. Acan, E. Aki-Sener, I. Yalcin, Some fused heterocyclic compounds as eukaryotic topoisomerase II inhibitors, Biochem. Biophys. Res. Commun. 317 (2004) 670–674.
[8] M. Ukei, M. Taniguchi, UK-1, a novel cytotoxic metabolite from streptomyces, sp. 517-02. III. Antibacterial action of demethyl UK-1, J. Antibiot. (Tokyo) 50 (9) (1997) 788–790.
[9] A. Varga, E. Aki-Sener, I. Yalcin, O. Temiz-Arpaci, B. Tekiner-Gulbas, G. Cherepnev, J. Molnar, Induction of apoptosis and necrosis by resistance modifiers benzazoles and benzoxazines on tumor cell line mouse lymphoma L5718 Mdr+ cells, In Vivo 19 (6) (2005) 1087–1091.
[10] F.C. Tenover, J.W. Biddle, M.V. Lancaster, Increasing resistance to vancomycin and other glycopeptides in staphylococcus aureus, Emerg. Infect. Dis. 7 (2001) 327–332.
[11] K. Poole, Multidrug resistance in gram-negative bacteria, Curr. Opin. Microbiol. 4 (2001) 500–508.
[12] K. Coleman, Recent advances in the treatment of gram-positive infections, Drug Discov. Today Ther. Strateg. 1 (2004) 455–460.
[13] D. Abbanat, M. Macielag, K. Bush, Novel antibacterial agents for the treatment of serious gram-positive infections, Expert Opin. Investig. Drugs 12 (2003) 379–399.
[14] S. Alper-Hayta, M. Arisoy, O. Temiz-Arpaci, I. Yildiz, E. Aki, S. Ozkan, F. Kaynak, Synthesis, antimicrobial activity, pharmacophore analysis of some new 2-(substitutedphenyl/benzyl)-5-[(2-benzofuryl)carboxamido]benzoxazoles, Eur. J. Med. Chem. 43 (2008) 2568–2578.
[15] I. Yildiz-Oren, B. Tekiner, I. Yalcin, O. Temiz-Arpaci, E. Aki-Sener, N. Altanlar, Synthesis and antimicrobial activity of new 2-[p-substituted-benzyl]-5-[substituted-carbonylamino] benzoxazoles, Arch. Pharm. 337 (7) (2004) 402–410.
[16] S. Armaković, S.J. Armaković, J.P. Šetrajčić, I.J. Šetrajčić, Active components of frequently used β-blockers from the aspect of computational study, J. Mol. Model 18 (2012) 4491–4501.
[17] B. Abramović, S. Kler, D. Šojić, M. Laušević, T. Radović, D. Vione, Photocatalytic degradation of metoprolol tartrate in suspensions of two TiO 2-based photocatalysts with different surface area. Identification of intermediates and proposal of degradation pathways, J. Hazard. Mater 198 (2011) 123–132.
[18] S.J. Armaković, S. Armaković, N.L. Finčur, F. Šibul, D. Vione, J.P. Šetrajčić, B. Abramović, Influence of electron acceptors on the kinetics of metoprolol photocatalytic degradation in TiO_2 suspension. A combined experimental and theoretical study, RSC Adv. 5 (2015) 54589–54604.
[19] M. Blessy, R.D. Patel, P.N. Prajapati, Y. Agrawal, Development of forced degradation and stability indicating studies of drugs-A review, J. Pharm. Anal. 4 (2014) 159–165.
[20] J. Molnar, J. Agbaba, B. Dalmacija, M. Klašnja, M. Watson, M. Kragulj, Effects of ozonation and catalytic ozonation on the removal of natural organic matter from groundwater, J. Environ. Eng. 138 (2011) 804–808.
[21] J.J. Molnar, J.R. Agbaba, B.D. Dalmacija, M.T. Klašnja, M.B. Dalmacija, M.M. Kragulj, A comparative study of the effects of ozonation and TiO 2-catalyzed ozonation on the selected chlorine disinfection by-product precursor content and structure, Sci. Total Environ. 425 (2012) 169–175.
[22] D.V. Šojić, D.Z. Orčić, D.D. Četojević-Simin, N.D. Banić, B.F. Abramović, Efficient removal of sulcotrione and its formulated compound Tangenta® in aqueous TiO 2 suspension: stability, photoproducts assessment and toxicity, Chemosphere 138 (2015) 988–994.
[23] D.V. Šojić, D.Z. Orčić, D.D. Četojević-Simin, V.N. Despotović, B.F. Abramović, Kinetics and the mechanism of the photocatalytic degradation of mesotrione in aqueous suspension and toxicity of its degradation mixtures, J. Mol. Catal. A Chem. 392 (2014) 67–75.
[24] D.D. Četojević-Simin, S.J. Armaković, D.V. Šojić, B.F. Abramović, Toxicity assessment of metoprolol and its photodegradation mixtures obtained by using different type of TiO 2 catalysts in the mammalian cell lines, Sci. Total Environ. 463 (2013) 968–974.
[25] P. Lienard, J. Gavartin, G. Boccardi, M. Meunier, Predicting drug substances autoxidation, Pharm. Res. 32 (2015) 300–310.
[26] G.L. de Souza, L.M. de Oliveira, R.G. Vicari, A. Brown, A DFT investigation on the structural and antioxidant properties of new isolated interglycosidic O-(1→ 3) linkage flavonols, J. Mol. Model 22 (2016) 1–9.
[27] Z. Sroka, B. Żbikowska, J. Hładyszowski, The antiradical activity of some selected flavones and flavonols. Experimental and quantum mechanical study, J. Mol. Model 21 (2015) 1–11.
[28] Clinical and Laboratory Standards Institute (CLSI), Performance Standards for Antimicrobial Disk Susceptibility Tests, Approved Standard, M2–A9 (formerly NCCLS), Clinical and Laboratory Standards Institute, 940 West Valley Road, Wayne, Pennsylvania, USA, 2006a.
[29] Clinical and Laboratory Standards Institute (CLSI), Performance Standards for Antimicrobial Susceptibility Testing, 16th Informational Supplement. CLSI M100-S16 (formerly NCCLS), Clinical and Laboratory Standards Institute, 940 West Valley Road, Wayne, Pennsylvania, USA, 2006b.
[30] M.J. Frisch, G.W. Trucks, H.B. Schlegel, G.E. Scuseria, M.A. Robb, J.R. Cheeseman, J.A. Montgomery Jr., T. Vreven, K.N. Kudin, J.C. Burant, J.M. Millam, S.S. Iyengar, J. Tomasi, V. Barone, B. Mennucci, M. Cossi, G. Scalmani, N. Rega, G.A. Petersson, H. Nakatsuji, M. Hada, M. Ehara, K. Toyota, R. Fukuda, J. Hasegawa, M. Ishida, T. Nakajima, Y. Honda, O. Kitao, H. Nakai, M. Klene, X. Li, J.E. Knox, H.P. Hratchian, J.B. Cross, C. Adamo, J. Jaramillo, R. Gomperts, R.E. Stratmann, O. Yazyev, A.J. Austin, R. Cammi, C. Pomelli, J.W. Ochterski, P.Y. Ayala, K. Morokuma, G.A. Voth, P. Salvador, J.J. Dannenberg, V.G. Zakrzewski, S. Dapprich, A.D. Daniels, M.C. Strain, O. Farkas, D.K. Malick, A.D. Rabuck, K. Raghavachari, J.B. Foresman, J.V. Ortiz, Q. Cui, A.G. Baboul, S. Clifford, J. Cioslowski, B.B. Stefanov, G. Liu, A. Liashenko, P. Piskorz, I. Komaromi, R.L. Martin, D.J. Fox, T. Keith, M.A. Al-Laham, C.Y. Peng, A. Nanayakkara, M. Challacombe, P.M.W. Gill, B. Johnson, W. Chen,

M.W. Wong, C. Gonzalez, J.A. Pople, Gaussian 03, Revision C.02, Gaussian, Inc., Wallingford CT, 2004.
[31] J.B. Foresman, in: E. Frisch (Ed.), Exploring Chemistry with Electronic Structure Methods: a Guide to Using Gaussian, Gaussian Inc., Pittsburg, PA, 1996.
[32] R. Dennington, T. Keith, J. Millam, GaussView. Version 5, Semichem Inc., Shawnee Mission, KS, 2009.
[33] J.M.L. Martin, C. Van Alsenoy, GAR2PED, a Program to Obtain a Potential Energy Distribution from a Gaussian Archive Record, University of Antwerp, Belgium, 2007.
[34] D. Shivakumar, J. Williams, Y. Wu, W. Damm, J. Shelley, W. Sherman, Prediction of absolute solvation free energies using molecular dynamics free energy perturbation and the OPLS force field, J. Chem. Theory Comput. 6 (2010) 1509–1519.
[35] Z. Guo, U. Mohanty, J. Noehre, T.K. Sawyer, W. Sherman, G. Krilov, Probing the α-helical structural stability of stapled p53 peptides: molecular dynamics simulations and analysis, Chem. Biol. Drug Des. 75 (2010) 348–359.
[36] K.J. Bowers, E. Chow, H. Xu, R.O. Dror, M.P. Eastwood, B.A. Gregersen, J.L. Klepeis, I. Kolossvary, M.A. Moraes, F.D. Sacerdoti, Scalable algorithms for molecular dynamics simulations on commodity clusters, in: SC 2006 Conference, Proceedings of the ACM/IEEE, IEEE, 2006.
[37] I. Fabijanić, C.J. Brala, V. Pilepić, The DFT local reactivity descriptors of α-tocopherol, J. Mol. Model 21 (2015) 1–7.
[38] A.D. Bochevarov, E. Harder, T.F. Hughes, J.R. Greenwood, D.A. Braden, D.M. Philipp, D. Rinaldo, M.D. Halls, J. Zhang, R.A. Friesner, Jaguar: a high-performance quantum chemistry software program with strengths in life and materials sciences, Int. J. Quantum Chem. 113 (2013) 2110–2142.
[39] A.D. Becke, Density-functional thermochemistry. III. The role of exact exchange, J. Chem. Phys. 98 (1993) 5648–5652.
[40] J.L. Banks, H.S. Beard, Y. Cao, A.E. Cho, W. Damm, R. Farid, A.K. Felts, T.A. Halgren, D.T. Mainz, J.R. Maple, Integrated modeling program, applied chemical theory (IMPACT), J. Comput. Chem. 26 (2005) 1752–1780.
[41] H.J. Berendsen, J.P. Postma, W.F. van Gunsteren, J. Hermans, Interaction models for water in relation to protein hydration, in: Intermolecular Forces, Springer, 1981, pp. 331–342.
[42] A. Otero-de-la-Roza, E.R. Johnson, J. Contreras-García, Revealing non-covalent interactions in solids: NCI plots revisited, Phys. Chem. Chem. Phys. 14 (2012) 12165–12172.
[43] E.R. Johnson, S. Keinan, P. Mori-Sanchez, J. Contreras-Garcia, A.J. Cohen, W. Yang, Revealing noncovalent interactions, J. Am. Chem. Soc. 132 (2010) 6498–6506.
[44] Schrödinger Release 2015-4: Maestro, Version 10.4, Schrödinger, LLC, New York, NY, 2015.
[45] K. Tamagawa, T. Iijima, M. Kimura, Molecular structure of benzene, J. Mol. Struct. 30 (1976) 243–253.
[46] R.T. Ulahannan, C.Y. Panicker, H.T. Varghese, R. Musiol, J. Jampilek, C. Van Alsenoy, J.A. War, A.A. Al-Saadi, Spectrochim. Acta 151 (2015) 335.
[47] J.B. Bhagyasree, J. Samuel, H.T. Varghese, C.Y. Panicker, M. Arisoy, O. Temiz-Arpaci, Synthesis, FT-IR investigation and computational study of 5-[(4-bromophenyl)acetamido]-2-(4-tert-butylphenyl)benzoxazole, Spectrochim. Acta 115 (2013) 79–91.
[48] C.Y. Panicker, H.T. Varghese, B. Narayana, K. Divya, B.K. Sarojini, J.A. War, C. Van Alsenoy, K.H. Fun, FT-IR, NBO, HOMO-LUMO, MEP analysis and molecular docking study of methyl N-({[2-(2-methoxyacetamido)-4-(phenylsulfanyl)phenyl] amino} [(methoxycarbonyl) imino]methyl) carbamate, Spectrochim. Acta 148 (2015) 29–42.
[49] R.T. Ulahannan, C.Y. Panicker, H.T. Varghese, R. Musiol, J. Jampilek, C. Van Alsenoy, J.A. War, S.K. Srivastava, Molecular structure, FT-IR, FT-Raman, NBO, HOMO and LUMO, MEP, NLO and molecular docking study of 2-[(E)-2-(2-bromophenyl)-ethenyl]quinoline-6-carboxylic acid, Spectrochim. Acta 151 (2015) 184–197.
[50] G. Socrates, Infrared Characteristic Group Frequencies, John Wiley and Sons, New York, 1981.
[51] (a) N.P.G. Roeges, A Guide to the Complete Interpretation of IR Spectra of Organic Compounds, Wiley, New York, 1994;
(b) G. Socrates, Infrared Characteristic Group Frequencies, John Wiley and Sons, New York, 1981.
[52] R.M. Silverstein, G.C. Bassler, T.C. Morril, Spectrometric Identification of Organic Compounds, fifth ed., John Wiley and Sons Inc., Singapore, 1991.
[53] Y.S. Mary, P.J. Jojo, C.Y. Panicker, C. Van Alsenoy, S. Ataei, I. Yildiz, Theoretical investigations on the molecular structure, vibrational spectra, HOMO-LUMO and NBO analysis of 5-chloro-2-((4-chlorophenoxy)methyl)benzimidazole, Spectrochim. Acta 122 (2014) 499–511.
[54] J.B. Bhagyasree, H.T. Varghese, C.Y. Panicker, J. Samuel, C. Van Alsenoy, K. Bolelli, I. Yildiz, E. Aki, Vibrational spectroscopic (FT-IR, FT-Raman,1H NMR and UV) investigations and computational study of 5-nitro-2-(4-nitrobenzyl) benzoxazole, Spectrochim. Acta 102 (2013) 99–113.
[55] N.B. Colthup, L.H. Daly, S.E. Wiberly, Introduction to IR and Raman Spectroscopy, Academic Press, New York, 1990.
[56] Y.S. Mary, P.J. Jojo, C.Y. Panicker, C. Van Alsenoy, S. Ataei, I. Yildiz, Quantum mechanical and spectroscopic (FT-IR, FT-Raman, 1H NMR and UV) investigations of 2-(phenoxymethyl)benzimidazole, Spectrochim. Acta 125 (2014) 12–24.
[57] S.H.R. Sebastian, M.A. Al-Alshaikh, A.A. El-Emam, C.Y. Panicker, J. Zitko, M. Dolezal, C. Van Alsenoy, Spectroscopic quantum chemical studies, Fukui functions, in vitro antiviral activity and molecular docking of 5-chloro-N-(3-nitrophenyl)pyarzine-2-carboxamide, J. Mol. Struct. 1119 (2016) 188–199.
[58] G. Varsanyi, Assignments of Vibrational Spectra of Seven Hundred Benzene Derivatives, Wiley, New York, 1974.
[59] R.I. Al-Wabli, K.S. Resmi, Y.S. Mary, C.Y. Panicker, M.A. Attia, A.A. El-Emam, C. Van Alsenoy, Vibrational spectroscopic studies, Fukui functions, HOMO-LUMO, NLO, NBO analysis and molecular docking study of (E)-1-(1,3-benzodioxol-5-yl)-4,4-dimethylpent-1-en-3-one, a potential precursor to bioactive agents, J. Mol. Struct. 1123 (2016) 375–383.
[60] V.V. Menon, E. Fazal, Y.S. Mary, C.Y. Panicker, S. Armakovic, S.J. Armakovic, S. Nagarajan, C. Van Alsenoy, FT-IR, FT-Raman and NMR characterization of 2-isopropyl-5-methylcyclohexyl quinoline-2-carboxylate and investigation of its reactive and optoelectronics properties by molecular dynamics simulations and DFT calculations, J. Mol. Struct. 1127 (2017) 124–137.
[61] Y.X. Sun, Q.L. Hao, W.X. Wei, Z.X. Yu, L.D. Lu, X. Wang, Y.S. Wang, Experimental and density functional studies on 4-(3,4-dihydroxy benzylideneamino) antipyrine and 4-(2,3,4-trihydroxybenzylideneamino)antipyrine, J. Mol. Struct. Theochem. 904 (2009) 74–82.
[62] A.S. El-Azab, Y.S. Mary, C.Y. Panicker, A.A.M. Abdel-Aziz, M.A. El-Sherbeny, C. Van Alsenoy, DFT and experimental (FT-IR and FT-Raman) investigation of vibrational spectroscopy and molecular docking studies of 2-(4-oxo-3-phenethyl-3,4-dihydroquinazolin-2-ylthio)-N-(3,4,5-trimethoxyphenyl)acetamide, J. Mol. Struct. 1113 (2016) 133–145.
[63] C. Adant, M. Dupuis, J.L. Bredas, Ab initio study of the nonlinear optical properties of urea : electron correlation and dispersion effects, Int. J. Quantum. Chem. 56 (1995) 497–507.
[64] E. Koscien, J. Sanetra, E. Gondek, B. Jarosz, I.V. Kityk, J. Ebothe, A.V. Kityk, Optical poling effect and optical absorption of cyan, ethylcarboxyl and tert-butyl derivatives of 1H-pyrazolo[3,4-b]quinoline, experiment and quantum chemical simulations, Spectrochim. Acta 61 (2005) 1933–1938.
[65] J.L. Gazquez, Perspectives of the density functional theory of chemical reactivity, J. Mex. Chem. Soc. 52 (2008) 3–10.
[66] P. Geerlings, F. De Profit, W. Langenaeker, Conceptual density functional theory, Chem. Rev. 103 (2003) 1793–1873.
[67] R.G. Parr, R.G. Pearson, Absolute hardness, companion parameter to absolute electronegativity, J. Am. Chem. Soc. 105 (1983) 7512–7516.
[68] R.G. Pearson, Recent advances in the concept of hard and soft acids and bases, J. Chem. Ed. 64 (1987) 561–567.
[69] R.G. Parr, P.K. Chattaraj, Principle of hardness, J. Am. Chem. Soc. 113 (1991) 1854–1855.
[70] R.G. Pearson, Absolute electronegativity and absolute hardness of Lewis acids and bases, J. Am. Chem. Soc. 107 (1985) 6801–6806.
[71] R.G. Parr, L. Szentpaly, S. Liu, Electrophilicity index, J. Am. Chem. Soc. 121 (1999) 1922–1924.
[72] J.S. Murray, J.M. Seminario, P. Politzer, P. Sjoberg, Average local ionization energies computed on the surfaces of some strained molecules, Int. J. Quantum Chem. 38 (1990) 645–653.
[73] P. Politzer, F. Abu-Awwad, J.S. Murray, Comparison of density functional and Hartree–Fock average local ionization energies on molecular surfaces, Int. J. Quantum Chem. 69 (1998) 607–613.
[74] A. Michalak, F. De Proft, P. Geerlings, R. Nalewajski, Fukui functions from the relaxed Kohn-Sham orbitals, J. Phys. Chem. 103A (1999) 762–771.
[75] NBO Version 3.1, E. D. Glendening, A. E. Reed, J. E. Carpenter, and F. Weinhold.
[76] X. Ren, Y. Sun, X. Fu, L. Zhu, Z. Cui, DFT comparison of the OH-initiated degradation mechanisms for five chlorophenoxy herbicides, J. Mol. Model 19 (2013) 2249–2263.
[77] L.-l. Ai, J.-y. Liu, Mechanism of OH-initiated atmospheric oxidation of E/Z-CF3CF= CFCF3: a quantum mechanical study, J. Mol. Model 20 (2014) 1–10.
[78] W. Sang-aroon, V. Amornkitbamrung, V. Ruangpornvisuti, A density functional theory study on peptide bond cleavage at aspartic residues: direct vs cyclic intermediate hydrolysis, J. Mol. Model 19 (2013) 5501–5513.
[79] J. Kieffer, É. Brémond, P. Lienard, G. Boccardi, In silico assessment of drug substances chemical stability, J. Mol. Struct. Theochem 954 (2010) 75–79.
[80] J.S. Wright, H. Shadnia, L.L. Chepelev, Stability of carbon-centered radicals: effect of functional groups on the energetics of addition of molecular oxygen, J. Comput. Chem. 30 (2009) 1016–1026.
[81] G. Gryn'ova, J.L. Hodgson, M.L. Coote, Revising the mechanism of polymer autoxidation, Org. Biomol. Chem. 9 (2011) 480–490.
[82] T. Andersson, A. Broo, E. Evertsson, Prediction of drug candidates' sensitivity toward autoxidation: computational estimation of c-h dissociation energies of carbon-centered radicals, J. Pharm. Sci. 103 (2014) 1949–1955.
[83] R.V. Vaz, J.R. Gomes, C.M. Silva, Molecular dynamics simulation of diffusion coefficients and structural properties of ketones in supercritical CO2 at infinite dilution, J. Supercritic. Fluids 107 (2016) 630–638.
[84] E.F.F. Cunha, E.F. Barbosa, A.A. Oliveira, C. Teodorico, A.A. Oliveira, T.C. Ramalho, Molecular modeling of mycobacterium tuberculosis DNA gyrase and its molecular docking study with gatifloxacin inhibitors DNA gyrase and its molecular docking study with gatifloxacin inhibitors, J. Biomol. Struct. Dyn. (March 2016) 1102, http://dx.doi.org/10.1080/07391102.2010.10508576, 2012.
[85] D.A. Ostrov, P.E. Corsino, K.A. Finton, N. Le, T.C. Rowe, Discovery of Novel DNA Gyrase Inhibitors by High-Throughput Virtual Screening, 51, 2007, pp. 3688–3698.
[86] K. Patel, C. Tyagi, S. Goyal, S. Jamal, D. Wahi, R. Jain, N. Bharadvaja, A. Grover, Identification of chebulinic acid as potent natural inhibitor of M.tuberculosis DNA gyrase and molecular insights into its binding mode of action, Comput.

Biol. Chem. 59 (2015) 37–47.
[87] V. Lamour, L. Hoermann, J.M. Jeltsch, P. Oudet, D. Moras, An open conformation of the thermus thermophilus gyrase B ATP-binding domain, J. Biol. Chem. 277 (2002) 18947–18953.
[88] O. Trott, A. Olson, AutoDock Vina: improving the speed and accuracy of docking with a new scoring function, efficient optimization, and multithreading, J. Comput. Chem. 31 (2010) 455–461.
[89] B. Kramer, M. Rarey, T. Lengauer, Evaluation of the FLEXX Incremental Construction Algorithm for Protein-ligand Docking, vol. 241, 1999, pp. 228–241.
[90] Accelrys Software Inc, Discovery Studio 3.5 Client, 2012.